Key Points:
- First comprehensive study of magnetic field data from all Galileo flybys of Callisto
- Induction signal from Callisto's subsurface ocean is observable only under very specific plasma conditions
- We provide encounter geometries for future Callisto flybys to detect magnetic signature of ocean

Correspondence to:
L. Liuzzo,
lucas.liuzzo@eas.gatech.edu

Magnetic signatures of plasma interaction and induction at Callisto: The Galileo C21, C22, C23, and C30 flybys

Lucas Liuzzo[1] (ID)**, Sven Simon[1]** (ID)**, Moritz Feyerabend[2]** (ID)**, and Uwe Motschmann[2,3]**

[1] School of Earth and Atmospheric Sciences, Georgia Institute of Technology, Atlanta, Georgia, USA, [2] Institute for Theoretical Physics, University of Braunschweig, Braunschweig, Germany, [3] Institute for Planetary Research, German Aerospace Center, Berlin, Germany

Abstract We apply a combination of analytical modeling, hybrid simulations, and data analysis techniques to provide a comprehensive study of magnetometer data from four Galileo flybys of Callisto (C21, C22, C23, and C30) that have never been discussed in the literature before. Callisto's distance to the center of Jupiter's magnetospheric current sheet varied considerably from flyby to flyby. Therefore, the relative strength of the magnetic field perturbations due to Callisto's plasma interaction with Jupiter's magnetosphere and induction within Callisto's subsurface ocean drastically changed as well. During C21, a strong magnetic field perturbation along the corotation direction was detected in Callisto's geometric plasma shadow. This enhancement can be explained with Callisto's steady state plasma interaction only, if the upstream flow possessed a nonnegligible component away from Jupiter. During C22, Galileo only grazed Callisto's Alfvén wings which were elevated out of the flyby plane due to the ambient magnetospheric field orientation. During C23, the combination of an inclined flyby trajectory and finite gyroradius effects caused Callisto's observed Alfvén wings to be slightly asymmetric between both hemispheres. During C30, a discontinuity with a surface normal pointed toward Jupiter was detected within Callisto's geometric plasma shadow, similar to the earlier C10 flyby. Due to strong plasma interaction and an unfavorable flyby geometry (C21), a large closest approach altitude (C22), or weak inducing field (C23 and C30), no discernible induction signatures were observed during these four flybys. Based on data from all available Galileo flybys, we determine requirements on future flyby geometries that must be satisfied for an identification of Callisto's subsurface ocean in magnetometer data.

1. Introduction

The four Galilean moons of Jupiter experience a time-varying magnetospheric background field, driven by the 9.6° tilt of Jupiter's magnetic moment with respect to its rotational axis. As a result of this tilt, Jupiter's magnetic equator and associated magnetospheric current sheet continually sweep through its rotational equatorial plane, where the orbits of the Galilean moons are located. At the icy moon Callisto, this effect is especially pronounced. Orbiting at a distance of 26.3 R_J (radius of Jupiter: $R_J = 71{,}492$ km), Callisto experiences variations of the magnetospheric field strength by an entire order of magnitude (4–40 nT) throughout a single synodic rotation (10.2 h), depending on the moon's magnetic latitude [*Kivelson et al.*, 2004].

With a radius of $R_C = 2410$ km, Callisto is the second largest of the Galilean moons and is thought to have an electrically conducting subsurface ocean at a depth of at most 300 km [*Zimmer et al.*, 2000]. Although Callisto is devoid of an internally generated dynamo field [*Khurana et al.*, 1997], the time-varying Jovian magnetospheric field induces currents within the ocean which manifest, to first order, as a dipolar magnetic field outside of the moon.

Carlson [1999] and recently *Cunningham et al.* [2015] have confirmed the presence of an atmosphere around Callisto that consists predominately of molecular oxygen and carbon dioxide. This atmosphere is partially ionized mainly by photoionization and electron impact ionization [e.g., *Kliore et al.*, 2002; *Strobel et al.*, 2002]. Once ionized, the newly generated charged particles are picked up by the magnetospheric electromagnetic fields and convected downstream. The gyroradii of the pickup ions are up to 10 times the size of Callisto and thus generate substantial asymmetries in the plasma and magnetic environment of the moon [*Liuzzo et al.*, 2015].

Callisto's orbital velocity around Jupiter is 8 km/s, compared to the approximately 200 km/s flow velocity of the ambient magnetospheric plasma that (nearly) corotates with the planet [*Kivelson et al.*, 2004]. As a result, the Jovian magnetospheric plasma and frozen-in magnetospheric field constantly overtake the moon and interact with its induced dipole and ionosphere. This interaction generates a compression of the induced dipole at Callisto's ramside, and the magnetic field piles up. In the moon's wake, the draped field lines form a bipolar magnetotail [*Liuzzo et al.*, 2015, 2016]. At larger distances from Callisto where the contribution of ionospheric currents to the magnetic field can be neglected, this draping forms two Alfvén wings that ultimately connect the moon with its parent planet's polar ionosphere [*Neubauer*, 1980, 1998]. This interaction of the Jovian magnetospheric plasma with Callisto partially obscures the electromagnetic induction signal generated in the subsurface ocean [*Zimmer et al.*, 2000; *Kivelson*, 2004; *Liuzzo et al.*, 2016]. The induction also has a feedback on the plasma interaction as it reduces the cross section of the Alfvén wings [*Neubauer*, 1999; *Volwerk et al.*, 2007]. Thus, Callisto's magnetic environment is characterized by a strong nonlinear coupling of induction and plasma interaction.

Which effect dominates the magnetic perturbations near Callisto at a given time depends on the distance of the moon from the center of Jupiter's magnetospheric current sheet. When Callisto is located away from the center of the current sheet induction dominates, and the induced field contributes approximately 80% of the overall magnetic perturbations near the moon [e.g., *Neubauer*, 1998; *Liuzzo et al.*, 2015]. However, when Callisto is located closer to the center of the Jovian current sheet, the plasma interaction dominates and may almost completely obscure any induction signal.

During the Galileo mission to the Jovian system between 1995 and 2003, Callisto's magnetic environment was observed during seven targeted flybys, denoted C3, C9, C10, C21, C22, C23, and C30. The magnetometer on board Galileo was not active near Callisto during the C20 flyby, which is therefore not relevant to this study.

Initial modeling attempts to identify the signature of Callisto's subsurface ocean in Galileo magnetometer data considered only induction in the moon's interior but neglected any currents associated with the plasma interaction. In this way, the magnetic field perturbations observed during the first two Galileo flybys of Callisto (C3 and C9) were successfully interpreted as the inductive response of a perfectly conducting layer beneath the moon's surface [*Khurana et al.*, 1998; *Kivelson et al.*, 1999; *Zimmer et al.*, 2000]. However, using a simple induction model for flybys other than C3 and C9 was shown to be unsuitable as currents generated by Callisto's plasma interaction were nonnegligible during the five remaining encounters.

The first to study Callisto's plasma interaction within the framework of a numerical simulation was *Seufert* [2012]. This author applied a magnetohydrodynamic (MHD) model to calculate the flow deflection and field line draping associated with the interaction between Jupiter's magnetospheric plasma and Callisto's ionosphere. However, these MHD simulations *did not* consider Callisto's induced dipole: *Seufert* [2012] simply added the dipole field to the output of the MHD model *after* the simulation had reached a stationary state. The important feedback between the plasma interaction and the induction effect was neglected, and the governing system of equations was not consistent.

Subsequently, *Lindkvist et al.* [2015] used a hybrid model to analyze the plasma interaction with Callisto's induced dipole. Consistent with *Zimmer et al.* [2000], these authors were able to reproduce Galileo magnetic field observations from the C3 and C9 flybys. However, since their model did not include the plasma interaction with Callisto's ionosphere, *Lindkvist et al.* [2015] were not able to explain Galileo data from the C10 encounter.

Recently, *Liuzzo et al.* [2016] were the first to study Callisto's magnetic and plasma environment with all relevant contributions included: induction in the subsurface ocean as well as plasma interaction with the moon's ionosphere and induced dipole. These authors analyzed magnetic field and plasma data from the Galileo C10 flyby of Callisto by using a combination of hybrid modeling and data analysis techniques. Their study was able to disentangle signatures in the C10 magnetometer data associated with the plasma interaction from those associated with induction. *Liuzzo et al.* [2016] identified two distinct magnetic regions near Callisto, dominated by either plasma interaction or induction. Outside of Callisto's geometric plasma shadow, the moon's magnetic environment was characterized by magnetic field pileup, field line draping, and the two Alfvén wings.

Within Callisto's geometric plasma shadow, *Liuzzo et al.* [2016] identified a quasi-dipolar "core region" directly downstream of the moon with an extension of approximately 1 R_C. The solid body of Callisto partially protects

this wakeside core region from the plasma interaction. In particular, the ionospheric plasma speed in that region is on the order of only 1 km/s [see *Strobel et al.*, 2002; *Liuzzo et al.*, 2015] and therefore much too small to cause any significant deformation of the dipole field. The nearly "uncontaminated" inductive response of the moon's subsurface ocean was therefore still visible in C10 magnetometer data from within this region. These two distinct magnetic regimes were separated by a rotational discontinuity, where the observed magnetic field vector rotated by approximately 50° over a spatial scale of only 0.09 R_C.

For the C10 flyby, the approach of *Liuzzo et al.* [2016] was successful in identifying the magnetic signature of Callisto's subsurface ocean in the complex admixture of plasma interaction and induction. Magnetometer data from the four remaining Callisto flybys (C21, C22, C23, and C30) may also include contributions from both induction and plasma interaction. However, the magnetic field data sets from these four Callisto flybys have not yet been subject to any modeling attempts. The goal of our study is therefore to identify the contributions of plasma interaction and induction to the magnetic field perturbations detected during the C21, C22, C23, and C30 encounters. In analogy to our preceding study [*Liuzzo et al.*, 2016], this will be accomplished through a combination of data analysis and hybrid modeling. Studying the magnetic field observations from the remaining Callisto encounters is particularly important since the impact of plasma currents on the visibility of the induction signal has so far been understood for only a *single* flyby, namely, C10.

In conjunction with our two preceding studies [*Liuzzo et al.*, 2015, 2016], the present work will create a comprehensive picture of Callisto's magnetic environment as observed during the Galileo era. Understanding the measured magnetic perturbations during the few available Callisto encounters is also useful for the upcoming JUICE (JUpiter ICy moons Explorer) mission that will include multiple flybys of the moon and aims to constrain properties (i.e., conductivity, thickness, and depth) of its subsurface ocean.

The structure of this study is as follows: the encounter geometries of the four remaining Callisto flybys are discussed in section 2, followed by a brief description of the hybrid simulation model (section 3). A flyby-to-flyby analysis of the observed magnetic field signatures follows in section 4, including comparisons of model results to Galileo magnetometer data. Finally, a brief summary of our major findings is given in section 5, along with a discussion of requirements on the geometries of spacecraft flybys that aim to identify Callisto's subsurface ocean in magnetometer data.

2. The Four Final Galileo Flybys of Callisto

Throughout the study, the Cartesian CphiO coordinate system is used. This system is centered at Callisto, with unit vector $\hat{\mathbf{x}}$ aligned with the corotational flow direction and $\hat{\mathbf{y}}$ pointed toward Jupiter. Unit vector $\hat{\mathbf{z}}$ is aligned with the Jovian spin axis and completes the right-handed set.

Figure 1 shows the trajectories of the four Galileo flybys studied (C21, C22, C23, and C30), projected onto the $x = 0$, $y = 0$, and $z = 0$ planes of the CphiO system. The location of the Sun during each flyby is denoted by a colored circle. All four encounters were wakeside passes, with their trajectories located within only 0.25 R_C of Callisto's equatorial ($z = 0$) plane. The trajectory of each flyby was slightly inclined toward upstream with respect to the spacecraft's direction of travel. During the C21 flyby, Galileo traveled from Callisto's Jupiter-averted ($y < 0$) hemisphere to its Jupiter-facing ($y > 0$) hemisphere. However, during the C22, C23, and C30 flybys, the spacecraft traveled from the moon's Jupiter-facing hemisphere into its Jupiter-averted hemisphere, as indicated by the arrows in Figure 1.

Table 1 includes information on the trajectory of each flyby. The closest approach (C/A) altitude of the spacecraft ranged from only 131.9 km (0.05 R_C) during C30 up to 2299.3 km (0.95 R_C) during C22. At C/A of the four flybys, Callisto's distance h_{cs} to the center of Jupiter's magnetospheric current sheet [see, e.g., *Smith et al.*, 1974, 1975] ranged from $h_{cs} = 0.87\,R_J$ north (C23) to $h_{cs} = -4.31\,R_J$ south (C22).

As discussed in section 1, the physics of Callisto's magnetic environment (plasma interaction versus induction) change as a function of $|h_{cs}|$. In our study, we give the physical effects precedence over the chronology of the flybys and therefore analyze the magnetic field observations in order of *decreasing* $|h_{cs}|$: C22 is discussed first in section 4.1, followed by C21 in section 4.2, C23 in section 4.3, and lastly C30 in section 4.4.

3. The Adaptive Ion-Kinetic, Electron-Fluid Hybrid Model

This study applies the *Adaptive Ion-Kinetic, Electron-Fluid* (AIKEF) hybrid model [*Müller et al.*, 2011] to Callisto's magnetic and plasma environment. AIKEF treats ions as particles and electrons as a massless,
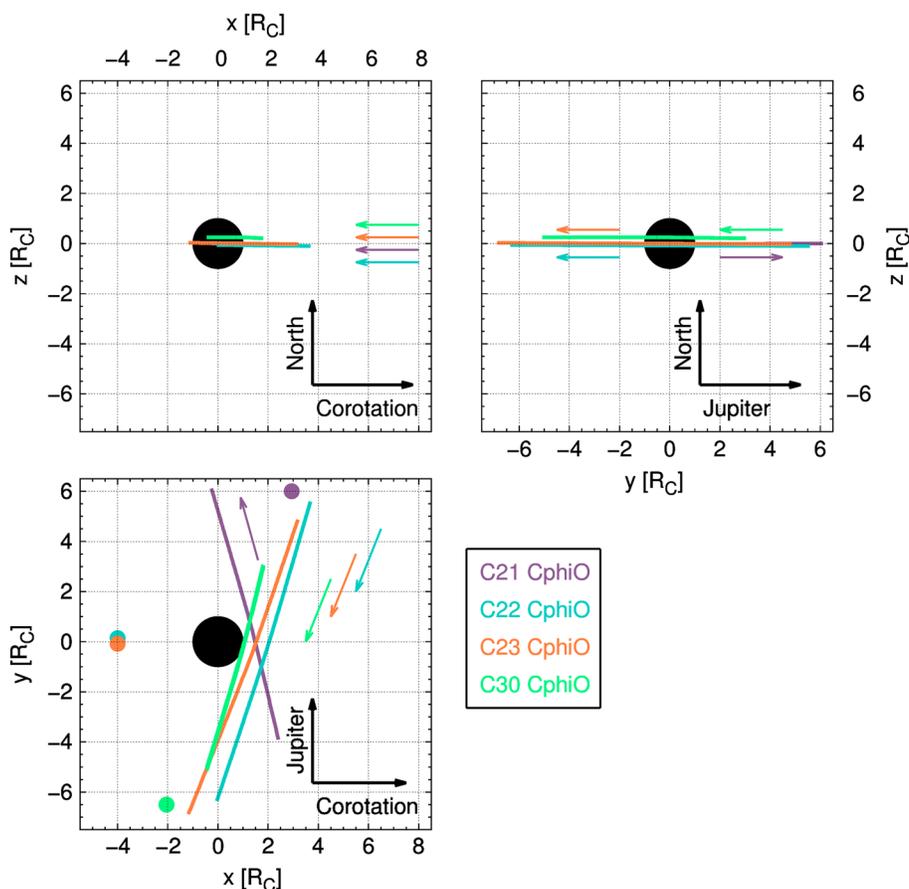
Figure 1. Projection of the (lavender) C21, (cyan) C22, (orange) C23, and (light green) C30 flyby trajectories onto the (clockwise from top left) $y = 0$, $x = 0$, and $z = 0$ planes of the CphiO coordinate system (see text). Colored arrows denote the travel direction of the Galileo spacecraft during each flyby. Colored circles correspond to the location of the Sun during each flyby.

charge-neutralizing fluid. A kinetic representation of the ions is required to study Callisto's interaction, as freshly generated O_2^+ and CO_2^+ pickup ions gyrate on spatial scales up to 10 times larger than the radius of the moon. Depending on Callisto's location with respect to the center of Jupiter's magnetospheric current sheet, the gyroradius of the impinging magnetospheric ions may also exceed the moon's radius by more than a factor of 3 [*Kivelson et al.*, 2004; *Liuzzo et al.*, 2015]. Capturing the resulting asymmetries in Callisto's plasma interaction is beyond the capabilities of any fluid model.

Table 1. The C21, C22, C23, and C30 Galileo Flybys of Callisto[a]

Flyby	Date	LT (h)	h_{cs} (R_J)	$d_{C/A}$ (km)	$d_{C/A}$ (R_C)
C21	30 Jun 1999	01:44	−1.87	1048.1	0.43
C22	14 Aug 1999	18:08	−4.31	2299.3	0.95
C23	16 Sep 1999	17:55	+0.87	1052.4	0.44
C30	25 May 2001	13:10	±0.00	131.9	0.05

[a]Dates of the flybys are included, with the local time of Callisto at closest approach (C/A) denoted by LT. The symbol h_{cs} represents the distance north ($h_{cs} > 0$) or south ($h_{cs} < 0$) of the center of Jupiter's magnetospheric current sheet at the time of C/A. Additionally, the C/A altitude of each flyby ($d_{C/A}$) in kilometers and Callisto radii ($R_C = 2410$ km) is included. This table has been adapted from *Liuzzo et al.* [2015].

AIKEF has already been used for extensive studies of Callisto's plasma environment. In particular, the model has been successfully applied to quantitatively explain Galileo magnetic field and plasma data from the C3, C9, and C10 flybys [*Liuzzo et al.*, 2015, 2016]. The plasma interaction of numerous Saturnian moons has also been studied with AIKEF, including most recently Titan [*Feyerabend et al.*, 2015, 2016] and Enceladus [*Kriegel et al.*, 2011, 2014]. Therefore, only a brief description of the model is given here. For a more detailed discussion, the reader is referred to those preceding works and references therein.

The modeled atmosphere surrounding Callisto consists of O_2 and CO_2 and is asymmetric between its ramside and wakeside hemispheres. Due to uncertainties in the processes that generate Callisto's atmosphere (sputtering versus sublimation), a day-night asymmetry of the atmosphere has also been tested in our earlier simulations for C3, C9, and C10, as well as in the simulations for the flybys presented in this study. However, consistent with the findings of *Liuzzo et al.* [2015], the magnetic signatures of Callisto's plasma interaction were nearly unchanged, regardless of whether a day-night or ram-wake asymmetry was applied. The implemented atmosphere model is consistent with the few available observations of Callisto's atmosphere, specifically those from the Galileo mission and several Hubble Space Telescope campaigns [see, e.g., *Carlson*, 1999; *Cunningham et al.*, 2015, and references therein]. For a more detailed discussion of the atmosphere model, the reader is referred to section 2.3 and Table 3 of *Liuzzo et al.* [2015].

Solar ultraviolet radiation and electron impacts ionize the neutral atmosphere to form an ionosphere around Callisto [e.g., *Kliore et al.*, 2002; *Strobel et al.*, 2002]. In the AIKEF model, the wavelength-dependent solar EUV flux model for aeronomic calculations [*Richards et al.*, 1994] is used to calculate photoionization rates, and energetic electrons are assumed to precipitate isotropically onto Callisto's atmosphere. The ionospheric plasma densities produced with this model were shown to be quantitatively consistent with Galileo measurements from the C10 flyby [*Liuzzo et al.*, 2016]. A complete description of the ionosphere model is available in *Liuzzo et al.* [2015, 2016].

Recently, *Hartkorn et al.* [2017] presented a three-dimensional fluid-kinetic model of Callisto's ionosphere that was able to explain all available radio occultation data from Galileo [*Kliore et al.*, 2002]. These authors showed that even when Callisto's dayside and ramside hemispheres do not coincide, an ionosphere is present in the moon's dayside hemisphere (see, e.g., Figure 10 in that work). This finding is consistent with Galileo plasma observations during the wakeside/dayside C3 flyby, which revealed cold plasma densities on the order of $100 \ cm^{-3}$ [*Gurnett et al.*, 1997]. Hybrid modeling results for the C3 flyby *without* an ionosphere around Callisto [*Lindkvist et al.*, 2015] showed a density increase to values less than $2 \ cm^{-3}$ in the moon's wake. However, hybrid simulations by *Liuzzo et al.* [2015] that included Callisto's ionosphere were able to generate densities on the order of $100 \ cm^{-3}$ downstream of Callisto, consistent with the C3 measurements. Moreover, for the C10 flyby (where Callisto's dayside and ramside hemispheres were also antialigned), analyses of plasma data by *Gurnett et al.* [2000] and *Liuzzo et al.* [2016] came to the same conclusion of an ionosphere at Callisto.

Only during the ramside/nightside C9 flyby the radio occultation measurements *did not* reveal any discernible ionosphere. *Hartkorn et al.* [2017] demonstrated that C9 was an isolated event during a time of very low solar flux (reduced by 35% compared to the other flybys with radio occultation data available). Therefore, the ionospheric density near Callisto's terminator (which was accessible to the radio occultation technique) may have been too low for detection. The studies of *Gurnett et al.* [1997, 2000], *Liuzzo et al.* [2015, 2016], and *Hartkorn et al.* [2017] disprove the hypothesis of *Kliore et al.* [2002] that an ionosphere is formed only when Callisto's dayside and ramside hemispheres coincide. Thus, the ionosphere is an omnipresent component of Callisto's plasma interaction that needs to be considered by any realistic model.

Liuzzo et al. [2015] systematically investigated the influence of Callisto's ionosphere on its magnetic environment for different relative orientations of the dayside and ramside hemispheres (denoted by the local time LT), and demonstrated that changes in the LT have only a minor quantitative influence on the magnetic perturbations near Callisto. A similar effect has been observed for the plasma interaction of Titan [*Ledvina et al.*, 2012] as well. However, the ionosphere *does* control the strength of the magnetic field perturbations in Callisto's Alfvén wings [*Liuzzo et al.*, 2016]. Therefore, *Lindkvist et al.* [2015], who did not include Callisto's ionosphere within their model, could not reproduce magnetic field data from the Galileo C10 flyby (for further discussion, see section 5, item 5 in *Liuzzo et al.* [2016]).

Assuming a spatially homogeneous but time-varying magnetospheric field $\mathbf{B}_0 = \left[B_{x,0}\hat{\mathbf{x}} + B_{y,0}\hat{\mathbf{y}} + B_{z,0}\hat{\mathbf{z}} \right]$ near closest approach as well as a spherically symmetric conducting ocean beneath Callisto's surface, the magnetic

Table 2. Hybrid Model Parameters for the C21, C22, and C23 Flybys[a]

Parameters	Flyby			
	C21		C22	C23
	Corotational ($\xi = 0°$)	Noncorotational ($\xi = 50°$)		
$\mathbf{B}_0$ (nT)	$-5.0\hat{\mathbf{x}} + 28.0\hat{\mathbf{y}} - 5.0\hat{\mathbf{z}}$	$-5.0\hat{\mathbf{x}} + 28.0\hat{\mathbf{y}} - 5.0\hat{\mathbf{z}}$	$7.0\hat{\mathbf{x}} + 31.4\hat{\mathbf{y}} - 11.0\hat{\mathbf{z}}$	$0.0\hat{\mathbf{x}} - 22.0\hat{\mathbf{y}} - 10.0\hat{\mathbf{z}}$
$\mathbf{u}_0$ (km/s)	$320.0\hat{\mathbf{x}}$	$205.7\hat{\mathbf{x}} - 245.1\hat{\mathbf{y}}$	$192.0\hat{\mathbf{x}}$	$192.0\hat{\mathbf{x}}$
$m_{i,0}$ (amu)	16 (O⁺)	16 (O⁺)	16 (O⁺)	16 (O⁺)
$n_{i,0}$ (cm⁻³)	0.25	0.25	0.05	0.30
$\beta_{i,0}$	0.362	0.362	0.005	0.058
M_A	1.02	1.02	0.23	0.86
M_{MS}	0.87	0.87	0.23	0.83
r_{g,O^+} (R_C)	0.77	0.77	0.39	0.55
r_{g,O_2^+} (R_C)	1.54	1.54	0.78	1.10
r_{g,CO_2^+} (R_C)	2.11	2.11	1.08	1.51
Box size	$-15\,R_C \leq x, y, z \leq +15\,R_C$	$-15\,R_C \leq x, y, z \leq +15\,R_C$	$-30\,R_C \leq x, y, z \leq +30\,R_C$	$-15\,R_C \leq x, y, z \leq +15\,R_C$
Maximum grid resolution (R_C)	0.06	0.06	0.05	0.05

[a]The magnetospheric background field at closest approach ($\mathbf{B}_0$) and upstream flow velocity vector ($\mathbf{u}_0$) are included, along with the upstream ion mass ($m_{i,0}$), number density ($n_{i,0}$), and plasma beta ($\beta_{i,0}$). The upstream plasma is assumed to consist of singly charged oxygen ions (see *Kivelson et al.* [2004] and *Liuzzo et al.* [2015, 2016] for discussion). The Alfvénic and magnetosonic Mach numbers of the upstream plasma are denoted by M_A and M_{MS}, respectively. Additionally, the gyroradii r_g of the upstream (O⁺) and the ionospheric (O_2^+ and CO_2^+) ion species are included for each simulation. Finally, the box size and maximum resolution of the hierarchical grid in the hybrid simulation [*Müller et al.*, 2011] are included in units of Callisto radii. The large box size has been chosen to prevent any impact of the outer boundary conditions on the plasma signatures near Callisto. Note that the size of the simulation domain is *much larger* than the regions shown in Figures 2, 3, and 5. Due to its small C/A altitude, no hybrid model results are presented for the C30 encounter (see discussion in section 4.4).

field $\mathbf{B}_{ind}$ induced within the moon's subsurface ocean can be represented by a dipole [*Zimmer et al.*, 2000]. Outside of Callisto, this induced field is given by

$$\mathbf{B}_{ind} = \frac{\mu_0}{4\pi r^5} \left[3 \left(\mathbf{r} \cdot \mathbf{M}_{ind} \right) \mathbf{r} - r^2 \mathbf{M}_{ind} \right] , \qquad (1)$$

where $\mathbf{r}$ is the vector from the center of Callisto to a point $\mathbf{r}$ outside of the moon at distance $r = |\mathbf{r}|$. The induced magnetic moment $\mathbf{M}_{ind}$ can be represented as

$$\mathbf{M}_{ind} = -\frac{2\pi R_C^3}{\mu_0} A e^{i\phi} \left(B_{x,0} \hat{\mathbf{x}} + B_{y,0} \hat{\mathbf{y}} \right) . \qquad (2)$$

In equation (2), the amplitude A and phase lag ϕ are determined by the conductivity, thickness, and depth of Callisto's subsurface ocean. *Khurana et al.* [1998], *Kivelson et al.* [1999], and *Zimmer et al.* [2000] modeled Galileo magnetometer data from the C3 and C9 flybys to show that when the plasma interaction is negligible, the inductive response of Callisto's subsurface ocean can be described by a perfectly conducting layer ($A = 1$) with no phase lag ($\phi = 0$). The analysis of *Liuzzo et al.* [2016] for the C10 flyby showed that when including the moon's plasma interaction, using $A = 1$ and $\phi = 0$ for the ocean is still consistent with Galileo magnetometer data. Similar to *Khurana et al.* [1998], *Kivelson et al.* [1999], *Zimmer et al.* [2000], and *Liuzzo et al.* [2016], we therefore again use $A = 1$ and $\phi = 0$ in the present study.

The timescale of Callisto's plasma interaction is much shorter than the period of the inducing magnetospheric field (minutes compared to hours, see, e.g., *Liuzzo et al.* [2015] and *Seufert et al.* [2011]). Therefore, the induced dipole at Callisto is treated as static throughout the course of a hybrid simulation. This approach is consistent with numerous preceding studies of plasma interaction and induction at the Galilean moons [e.g., *Zimmer et al.*, 2000; *Rubin et al.*, 2015; *Lindkvist et al.*, 2015; *Liuzzo et al.*, 2015, 2016, and references therein].

Multiple simulations for each Callisto flyby have been performed by systematically varying the incident magnetospheric flow conditions. However, only a representative selection of the most insightful runs for each flyby is presented in this study. Table 2 lists the upstream plasma parameters for the included model runs, along with relevant numerical parameters of the hybrid simulations. The chosen upstream parameters are within the range of measured values at Callisto's orbital distance [*Kivelson et al.*, 2004]. However, the specific upstream

plasma moments at the time of each Callisto flyby are not available in the peer-reviewed literature. For this reason, the upstream conditions in the hybrid simulations are partially used as free parameters to adjust the modeled plasma interaction signatures to Galileo magnetometer observations.

The parameter space that needs to be explored for each of these remaining flybys is vast and—apart from magnetic field data—not constrained through plasma observations on a flyby-to-flyby basis. Therefore, we *do not* expect to achieve agreement between model output and all observed magnetic field signatures. Rather, we use output from a number of selected simulations as a guide to isolate the plasma interaction features from those signatures generated by induction.

4. Results and Discussion

4.1. The C22 Flyby

The Galileo C22 flyby of Callisto occurred on 14 August 1999 (see Table 1). With a closest approach (C/A) altitude of $d_{C/A} = 2299.3$ km $= 0.95\,R_C$, the C22 flyby was the most distant of all Galileo flybys. During this encounter, Callisto was located at a distance of $h_{cs} = -4.31\,R_J$ south of the center of the Jovian magnetospheric current sheet, which was the largest value during any of the Callisto flybys. At this distance, the magnetic signal of induction is expected to clearly dominate over the plasma interaction signatures [see, e.g., *Kivelson et al.*, 1999; *Zimmer et al.*, 2000; *Liuzzo et al.*, 2015].

Figure 2a shows the B_x, B_y, and B_z components as well as the total magnetic field $|\mathbf{B}|$ near Callisto for ± 30 min around C/A of the C22 flyby. The solid vertical black line denotes the time of closest approach, while the dashed vertical black lines represent the location of Callisto's geometric plasma shadow (defined by $\sqrt{y^2 + z^2} \leq 1\,R_C$ and $x > 0\,R_C$). Depicted in black are the magnetic field components measured by Galileo.

The measured magnetic field was only slightly perturbed during the C22 flyby. These perturbations included three regions that displayed a weak increase in B_x of approximately 5 nT above the magnetospheric background value of $B_{x,0} \approx 7$ nT (labeled I, II, and III in Figure 2a). As is visible in Figure 2a, the first of these segments (I) began before entering Callisto's geometric plasma shadow and continued to before C/A (from 08:15 to 08:26). The second (II) and third (III) segments were observed at the outbound edge of the moon's geometric plasma shadow, between 08:33 and 08:41 and between 08:41 and 08:50, respectively. The B_z perturbations in segments I and II were anticorrelated to the B_x perturbations: B_z decreased from $B_{z,0} \approx -11$ nT to $B_z \approx -15$ nT on both sides of the plasma shadow. The B_y component displayed only weak, short-scale fluctuations on the order of 10% of the background value ($B_{y,0} \approx 30$ nT). If any of these observed magnetic field perturbations were generated by Callisto, they would represent the weakest interaction signatures of the moon during all of the Galileo flybys [cf. *Kivelson et al.*, 1999; *Zimmer et al.*, 2000; *Liuzzo et al.*, 2016].

During the C22 flyby, the magnetospheric background field was weakly inhomogeneous (see Figure 2a). In the AIKEF model, this inhomogeneity is included by using the expression

$$\mathbf{B}_0 = \left[7.00\hat{\mathbf{x}} + \left(-\frac{0.88y}{R_C} + 30.91 \right)\hat{\mathbf{y}} + \left(\frac{0.88z}{R_C} - 10.90 \right)\hat{\mathbf{z}} \right] \text{nT} \tag{3}$$

for the background field, thereby ensuring $\nabla \cdot \mathbf{B}_0 = 0$ within the simulation. A similar treatment of the magnetospheric field was used by *Liuzzo et al.* [2016] for the C10 flyby. At closest approach of C22, the background field reads $\mathbf{B}_0 = \left[7.00\hat{\mathbf{x}} + 31.44\hat{\mathbf{y}} - 10.97\hat{\mathbf{z}} \right]$ nT and forms an angle of about 19° with the $z = 0$ plane. According to equation (2), this background field corresponds to $\mathbf{M}_{ind} = \left[-0.48\hat{\mathbf{x}} - 2.20\hat{\mathbf{y}} \right] \cdot 10^{18}$ Am^2. The induced dipole is thus rotated by an angle of 12° clockwise against the $-y$ axis. The value of $|\mathbf{M}_{ind}| = 2.25 \cdot 10^{18}$ Am^2 similar to those calculated by *Zimmer et al.* [2000] for C3 ($|\mathbf{M}_{ind}| = 2.22 \cdot 10^{18}$ Am^2) and C9 ($|\mathbf{M}_{ind}| = 2.36 \cdot 10^{18}$ Am^2) and by *Liuzzo et al.* [2016] for C10 ($|\mathbf{M}_{ind}| = 2.42 \cdot 10^{18}$ Am^2).

At the "magnetic poles" of Callisto (i.e., $x \approx 0$, $y = \pm 1\,R_C$, and $z = 0$), the induced magnetic moment for C22 results in a maximum surface field strength of 32.21 nT. However, due to the r^{-3} dependence of the induced dipole, the maximum observable field strength at an altitude of $d_{C/A} = 0.95\,R_C$ above the moon's magnetic poles would have been $|\mathbf{B}_{ind,max}| = 4.32$ nT. Therefore, the ratio of Callisto's induced field to the magnetospheric background field could not have exceeded 13% at this altitude. This value is too small for the magnetic signature of the moon's subsurface ocean to be clearly identifiable over the $\approx 10\%$ fluctuations of the magnetospheric background field observed throughout the entire flyby. Additionally, the geometry of the C22 trajectory prevented the spacecraft from passing near Callisto's magnetic poles where $|\mathbf{B}_{ind}|$ maximizes. The blue lines in Figure 2a, which show the magnetic field signature along the C22 trajectory generated

Figure 2. (a) Magnetic field signatures during the C22 flyby with (black) Galileo magnetometer data, (blue) the pure inductive response of Callisto's subsurface ocean, and (red) the combination of induction and plasma interaction from the AIKEF hybrid model. The solid black line at 08:30:52 denotes the closest approach time of Galileo, and the dashed lines denote the outer edges of Callisto's geometric plasma shadow. From top to bottom are B_x, B_y, B_z, $|\mathbf{B}|$, and electron number density n_e. Since there is no time series for the observed n_e available in the literature, only the electron number density from the hybrid model is shown in red. Regions I, II, and III are highlighted in light blue (see text for discussion). Two-dimensional profiles of (b) B_x, (c) B_y, and (d) B_z in Callisto's equatorial ($z = 0$) plane from the hybrid simulation. The projection of the C22 flyby trajectory onto this plane is included. Modeled (e) electron number density and (f) ionospheric O_2^+ number density in Callisto's equatorial ($z = 0$) plane, and (g) ionospheric O_2^+ number density in Callisto's polar ($y = 0$) plane. Note the difference in color scale between the densities of the electrons and the ionospheric ions. The color scales are intentionally oversaturated in Callisto's ionosphere to highlight smaller, more complex density structures in the moon's pickup tail.

by the induced dipole alone (see equations (1) and (2)), clearly demonstrate that identification of the induction effect was not feasible in magnetometer data from this flyby. In other words, although a strong induction signal should have been present at the time of C22, the large C/A altitude prevented detection of this signature.

We now investigate whether Callisto's plasma interaction (with the combined dipole-ionosphere obstacle) made any measurable contributions to the magnetic signatures observed during the C22 encounter. Figures 2b–2d show two-dimensional color plots of the modeled B_x, B_y, and B_z components in Callisto's $z = 0$ plane (which also contains the moon's induced magnetic moment) obtained from the hybrid simulation. The B_x signatures in the immediate vicinity of Callisto (see Figure 2b) are mainly generated by the induced dipole. The induced field lines leave Callisto in its Jupiter-averted ($y < 0$) hemisphere and return to the moon in its Jupiter-facing ($y > 0$) hemisphere. A "shamrock"-like structure is visible in Figure 2b, with regions of (red) increased B_x where the field points toward downstream and regions of (blue) decreased B_x where the field points toward upstream. The background value $B_{x,0} \approx 7$ nT is depicted in white. The induced dipole is only weakly affected by the plasma interaction: at the ramside of Callisto ($x < 0$), the induced field is slightly compressed and the two "shamrock leaves" are convected toward downstream. The two dipole "leaves" in B_x emerging from Callisto's wakeside hemisphere ($x > 0$) are also slightly stretched along the corotation direction.

Along the Galileo trajectory, the plasma interaction effectively increases the strength of the B_x perturbations generated by the induced dipole. This is visible in Figure 2a from 08:20 to 08:41. While in this region the pure dipole (blue line) shows only a weak, bipolar B_x signature, the plasma interaction (red line) enhances B_x symmetrically around the $y = 0$ line. The slight B_x enhancement detected within segment II of Figure 2a might therefore have been generated by stretching of the induced dipole due to the plasma interaction. This feature arises from the deformation of the positive B_x shamrock leaf in Callisto's wake, as visible in Figure 2b. However, the modeled decrease in B_x associated with the plasma interaction in segment I was not observed by Galileo, which instead detected an increase at this location. In segment III, Galileo detected an increase in B_x, while the model suggests no perturbation. We have carried out multiple simulations with different sets of upstream parameters within the regime proposed by *Kivelson et al.* [2004]. However, we did not find a parameter combination that produced a similar B_x perturbation as detected by Galileo in regions I and III.

The weakly inhomogeneous magnetospheric background field is mainly visible in Figure 2c, which depicts the modeled B_y: over a distance of 16 R_C, the B_y component changes by nearly 15 nT. Since the background field is antialigned with Callisto's induced magnetic moment, the B_y component near the moon's magnetic poles is reduced (depicted in blue). However, B_y is also reduced near Callisto's "magnetic equator" (near $y \approx 0$), since the ambient magnetospheric field is partially prevented from penetrating into Callisto's ionosphere [see also *Liuzzo et al.*, 2015]. Above the ionosphere, the magnetospheric field weakly piles up against the obstacle, as visible at the ramside of Callisto from $-3\,R_C \leq x \leq -1.4\,R_C$ in Figure 2c. The slightly negative B_y perturbations measured by Galileo after exiting Callisto's geometric plasma shadow (segment II in Figure 2a) were probably generated by the interaction of the induced dipole with Jupiter's magnetospheric plasma. Similar to the B_x signature in that region, the plasma interaction results in a slightly stronger magnetic perturbation than the pure dipole alone.

As Callisto's induced magnetic moment is confined to the moon's equatorial plane, the modeled B_z component in Figure 2d shows no dipolar signatures. Rather, the modeled perturbations in this component are mainly associated with Callisto's weak Alfvén wings. The directions of the two Alfvén wing characteristics $\mathcal{Z}^\pm$ can be calculated from

$$\mathcal{Z}^\pm = \mathbf{u}_0 \pm \mathbf{v}_{A,0} \quad , \tag{4}$$

where $\mathbf{u}_0$ is the upstream magnetospheric bulk velocity and $\mathbf{v}_{A,0}$ is the Alfvén velocity in the undisturbed magnetospheric plasma [*Neubauer*, 1980]. By inserting the upstream parameters from Table 2 into equation (4), Callisto's Jupiter-facing wing ($\mathcal{Z}^+$, extending into the $y > 0$ half-space) is found to be rotated out of the moon's equatorial plane into the $z < 0$ hemisphere by an angle of 17.5°. Callisto's Jupiter-averted wing ($\mathcal{Z}^-$, extending into the $y < 0$ half-space) is found to form an angle of 19.2° with the equatorial plane and is rotated into the moon's $z > 0$ hemisphere. Both wings are inclined by an angle of 12.2° with respect to the background field $\mathbf{B}_0$ [see *Neubauer*, 1980, equation (4)]. At larger distances to Callisto (well outside of the modeled simulation domain) the Jupiter-facing Alfvén wing connects the moon to Jupiter's south polar ionosphere, while the Jupiter-averted wing connects the moon to Jupiter's north polar ionosphere.

In Figure 2d, the weak positive B_z perturbation (depicted in red, extending into the $y > 0$ hemisphere) corresponds to Callisto's Jupiter-facing (southern) Alfvén wing. The slightly larger angle between Callisto's equatorial plane and the moon's Jupiter-averted (northern) Alfvén wing (19.2° compared to 17.5°) results in an even weaker magnetic signature of the Jupiter-averted wing (depicted in blue, extending into the $y < 0$ hemisphere) in this plane. The B_z perturbations associated with the Alfvén wings do not exceed 10% of the background field strength; i.e., they are much weaker than the modeled perturbations in B_x and B_y. We refrain from showing slices through the planes defined by $\mathbf{u}_0$ and $\mathcal{Z}^{\pm}$, as the respective magnetic signatures are very similar to those already shown in [*Liuzzo et al.*, 2015, 2016].

Hence, the hybrid model suggests that Galileo simply missed the central regions of Callisto's already weak Alfvén wings during the C22 flyby. Rather, the spacecraft grazed the outer regions of the wings where the draped magnetic field lines close [e.g., *Simon et al.*, 2011, Figure 8]. In segment II of the C22 trajectory, the modeled decrease of B_z is in qualitative agreement with Galileo data but is much weaker than the observed perturbation. In segment I, however, the model shows no discernible B_z perturbations which is consistent with the interpretation of the observed B_x and B_z signatures in this region being magnetospheric in origin and unrelated to Callisto. Neither the hybrid model nor the observations show any B_z perturbation in segment III.

The *increase* of B_x visible in segment III was accompanied by a simultaneous *decrease* of B_y, while B_z and $|\mathbf{B}|$ remained nearly constant. Thus, Galileo observed a *rotation* of the magnetic field vector in that region. This feature may have been associated with a traveling magnetospheric Alfvén wave that was encountered near Callisto. Alternatively, if the incident magnetospheric flow conditions were not stationary during C22, a slight change in the direction of the upstream velocity $\mathbf{u}_0$ may have pushed the Jupiter-averted Alfvén wing into the path of the Galileo spacecraft.

Shown in Figures 2e and 2f are the modeled electron number density n_e and ionospheric O_2^+ number density in Callisto's equatorial ($z = 0$) plane. Figure 2g displays the ionospheric O_2^+ number density in the moon's polar ($y = 0$) plane. The density structure of the ionospheric CO_2^+ ions is not shown as this population is less dense than O_2^+ by more than an order of magnitude. Therefore, the CO_2^+ ions act only as test particles that do not have a discernible effect on the magnetic field [see *Liuzzo et al.*, 2015]. The asymmetries associated with the large O_2^+ ion gyroradii (on the order of 1 R_C; see Table 2) are mainly visible in planes perpendicular to the background magnetic field (see Figure 2g). For C22, the density structures in the $z = 0$ plane are therefore nearly symmetric between the $y < 0$ and $y > 0$ hemispheres of the moon (Figure 2f). The slight shift of the tail into the $y < 0$ half-space is generated by the positive $B_{x,0}$ component of the background field *Simon and Motschmann* [2009]. In Callisto's equatorial wake, the escaping O_2^+ ions are confined to a narrow outflow channel located within $y = \pm 2 R_C$. The apparent fragmentation of the pickup tail visible in Figure 2f is caused by the asymmetric, "wavy" structure of the tail perpendicular to $\mathbf{B}_0$, which is visible in the $y = 0$ plane (see Figure 2g).

The electron density displayed in Figure 2e also shows a channel-like enhancement in Callisto's wake. The modeled electron density reaches a maximum value of $n_e \approx 0.3$ cm^{-3} along the flyby trajectory just before C/A (see Figure 2a, fifth panel). While there is no time series of the measured electron density available for C22, *Gurnett et al.* [2000] were able to use plasma wave data to obtain an estimate for the electron density in Callisto's geometric plasma shadow of approximately $n_e = 0.21$ cm^{-3}. This value is in reasonable agreement with both the magnitude and the location of the peak value obtained from the hybrid model along the flyby trajectory.

During the earlier C10 encounter, Galileo detected electron density enhancements on the order of $n_e \approx 400$ cm^{-3} in Callisto's geometric plasma shadow, which was successfully reproduced by the hybrid model of *Liuzzo et al.* [2016]. This enhancement was attributed to strong plasma outflow from the moon's ionosphere during the C10 flyby [*Gurnett et al.*, 2000; *Liuzzo et al.*, 2016]. During C22, there was no enhancement of the electron density measured in Callisto's wake that was even remotely as strong as during the C10 encounter. However, the maximum modeled electron density along the C22 flyby trajectory of $n_e \approx 0.3$ cm^{-3} is not only in agreement with plasma observations but is also consistent with ionospheric occultation measurements from Galileo that suggest the presence of an ionosphere surrounding Callisto at the time of this flyby [*Kliore et al.*, 2002]. The discrepancy in observed electron densities between these two flybys may therefore be associated with the much weaker plasma interaction during C22 compared to C10 [cf. *Liuzzo et al.*, 2016].

We also note that during C22, Callisto's dayside hemisphere coincided with its ramside hemisphere, whereas both hemispheres were nearly antialigned during C10. Thus, during C22, the bulk of the ionospheric plasma

needed to circumnavigate Callisto, which may also contribute to the lower plasma density directly downstream of the moon compared to C10. At the time of the C22 flyby, Callisto's magnetic environment was dominated by the induced dipole and currents associated with the plasma interaction were weak (due to the large distance to the center of Jupiter's current sheet). Therefore, the ionosphere made only a minor contribution to the already weak Alfvén wings (on the order of 10% of $\mathbf{B}_0$; see Figure 2d).

4.2. The C21 Flyby

The Galileo C21 flyby of Callisto occurred on 30 June 1999, with a closest approach altitude of $d_{C/A} = 1048.1$ km (0.43 R_C). At the time of this flyby, Callisto was located at a distance of $h_{cs} = -1.87\,R_J$ south of the center of Jupiter's magnetospheric current sheet. Hence, the magnetic moment induced within Callisto's subsurface ocean was only slightly weaker than for the C10 flyby ($h_{cs} = -2.45\,R_J$). The trajectory of the C21 flyby was similar to that of C10, with the spacecraft traveling from Callisto's $y < 0$ hemisphere into its $y > 0$ hemisphere (see Figure 1).

Displayed in Figure 3a are the magnetic field components (black) measured by Galileo during C21. As with Figure 2a, the vertical dashed lines correspond to the outer edges of Callisto's geometric plasma shadow, and the vertical solid line denotes the closest approach of the spacecraft. The nonconstant magnetospheric background field has been subtracted in Figure 3a to improve visibility of the magnetic perturbations that were observed during the flyby. These perturbations above or below the background value are denoted by $\delta B_{x,y,z}$ (i.e., the perturbations $\delta B_{x,y,z}$ are centered around a baseline value of 0). Magnetic field data for C21 with the background field included are shown in Figure 6 of *Liuzzo et al.* [2016] and are therefore not included here again.
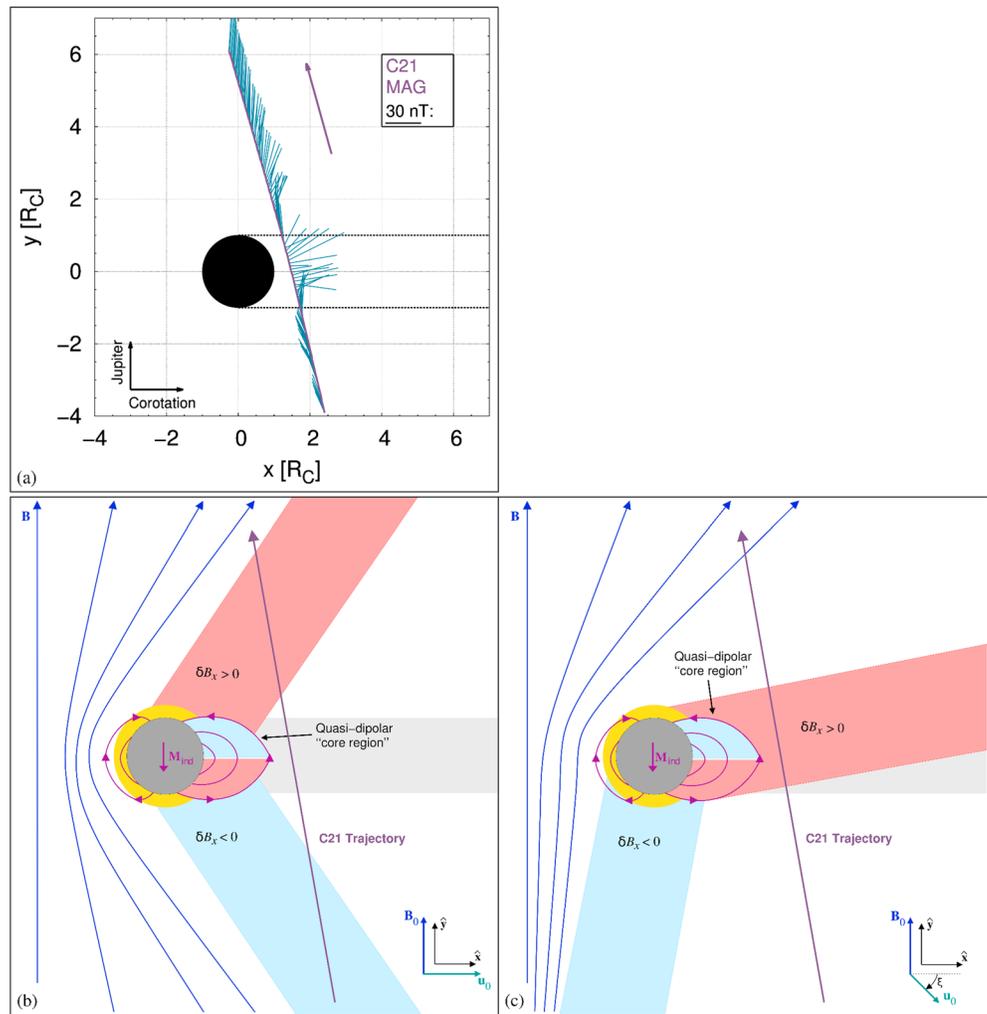
The magnetospheric background field at closest approach was $\mathbf{B}_0 = \left[-5.0\hat{\mathbf{x}} + 28.0\hat{\mathbf{y}} - 5.0\hat{\mathbf{z}}\right]$ nT, with $|\mathbf{B}_0| = 28.9$ nT. Thus, the background field is inclined by only 10° against the y axis and also forms an angle of only about 10° with the $z = 0$ plane. For our physical interpretation we can therefore, in good approximation, assume that $\mathbf{B}_0$ is (nearly) parallel to the positive y axis. The observed magnetic field projected onto Callisto's equatorial ($z = 0$) plane can be seen in Figure 4a.

The magnetic field displayed strong perturbations during the C21 wake passage with magnitudes of approximately 20–30 nT in all three components (Figure 3a). The most peculiar feature is the substantial increase of B_x detected within Callisto's geometric plasma shadow between 07:41 and 07:49, as visible in Figures 3a and 4a. An *M*-like feature is clearly visible in that region, with the maximum perturbation $\delta B_{x,\mathrm{max}}$ comparable to $|\mathbf{B}_0|$ at closest approach (i.e., $\delta B_{x,\mathrm{max}}/|\mathbf{B}_0| \approx 1$). As is demonstrated in Figure 4a, the magnetic field nearly pointed toward downstream in that region. Compared to other wakeside Callisto flybys with similar C/A altitudes, the next largest perturbation of $\delta B_{x,\mathrm{max}}/|\mathbf{B}_0| \approx 0.36$ was observed during the C23 flyby (see section 4.3). The B_x increase measured during C21 is rather anomalous for Callisto's geometric plasma shadow: a strong magnetic field component aligned with the corotation direction usually indicates field line draping. However, the results of *Liuzzo et al.* [2015, 2016] suggest that even for high Alfvénic Mach numbers (i.e., $M_A \gg 1$) the draped field lines do not penetrate significantly into Callisto's plasma shadow.

During the C21 flyby, the sequence of the detected B_x perturbations (see Figure 3a) was qualitatively similar to those observed during the C10 flyby [*Liuzzo et al.*, 2016]. During both encounters, a $\delta B_x < 0$ signature was detected inbound of Callisto's geometric plasma shadow. This decrease was followed by a $\delta B_x > 0$ segment and a subsequent $\delta B_x < 0$ segment while Galileo was in the moon's plasma shadow. Finally, after exiting the shadow, a region of $\delta B_x > 0$ was encountered, before B_x returned to its background value (i.e., $\delta B_x = 0$). For the C10 flyby, *Liuzzo et al.* [2016] found that this sequence of δB_x features corresponded to two distinct regions of Callisto's magnetic environment: outside of Callisto's plasma shadow, the moon's plasma interaction dominated, generating field line draping and Alfvén wings. Within the geometric plasma shadow, induction in Callisto's subsurface ocean dominated the observed magnetic field and the quasi-dipolar core region, partially protected from the plasma interaction, was visible [see *Liuzzo et al.*, 2016, Figure 4a]. However, the four δB_x features seen during C10 were all approximately of the same magnitude. For the C21 flyby, the δB_x enhancement within Callisto's plasma shadow (from 07:41 to 07:49) was anomalously strong compared to the other three perturbations (i.e., $\delta B_x < 0$ from 07:32 to 07:41, $\delta B_x < 0$ from 07:48 to 07:53, and $\delta B_x > 0$ from 07:53 to 07:58; see Figure 3a).

To determine whether the large $\delta B_x > 0$ enhancement seen in the geometric plasma shadow during C21 was related to Callisto's wakeside quasi-dipolar core region, we evaluate the contribution of the induced dipole

Figure 3. (a) Magnetic field signatures for the C21 flyby trajectory (black) measured by the Galileo spacecraft, and (blue) of a pure dipole induced within Callisto's subsurface ocean. Hybrid model results for the simulation with upstream flow (red) aligned with corotation (i.e., with $\xi = 0°$) and (dark green) offset by an angle of $\xi = 50°$ away from Jupiter are included. The background field $\mathbf{B}_0$ has been removed from the data (see text), and the symbol δ denotes perturbations above or below the background values. The vertical lines represent the (solid) time of closest approach and the (dashed) outer edges of Callisto's geometric plasma shadow. The turquoise feature within the shadow is discussed in the text. Two-dimensional color plots of (b) δB_x, (c) δB_y, and (d) ionospheric O_2^+ number density in Callisto's equatorial ($z = 0$) plane from the "corotational" hybrid simulation ($\xi = 0°$). The projection of the C21 flyby trajectory onto this plane is included. Two-dimensional color plots of (e) δB_x, (f) δB_y, and (g) ionospheric O_2^+ number density in Callisto's equatorial ($z = 0$) plane from the "noncorotational" hybrid simulation ($\xi = 50°$).

Figure 4. A possible explanation for the anomalous B_x increase observed in Callisto's geometric plasma shadow during C21. (a) A projection of the measured magnetic field vectors along the flyby trajectory onto the $z = 0$ plane. Callisto's geometric plasma shadow is denoted by the dotted bold lines that extend toward downstream. The magnetic field vectors are plotted every 24 s. (b, c) Schematic of the magnetic field orientation near Callisto in the $z = 0$ plane for an upstream flow (Figure 4b) in the direction of corotation (i.e., with $\xi = 0°$) and (Figure 4c) offset by an angle $\xi > 0$ into the Jupiter-averted hemisphere. Callisto's induced magnetic moment and resulting dipolar field lines are depicted in magenta. The associated quasi-dipolar core region is depicted at Callisto's wakeside well below the trajectory of the (lavender line) C21 flyby. Magnetic field lines (blue) drape to form Alfvén wings and generate perturbations of (red) positive δB_x above and (blue) negative δB_x below the background value. The moon's geometric plasma shadow is shaded light gray. Note that the figure *is not* to scale, especially regarding the quasi-dipolar core region, Callisto's ionosphere and induced magnetic field, and the location of the flyby trajectory.

to the magnetic field along the C21 trajectory. Using the magnetospheric background field $\mathbf{B}_0$ around C/A of C21, equation (2) yields an induced magnetic moment of $\mathbf{M}_{ind} = \left[0.35\hat{\mathbf{x}} - 1.96\hat{\mathbf{y}}\right] \cdot 10^{18}$ Am^2 that is tilted by only 10° against the $-y$ axis. As Callisto's distance to the center of Jupiter's current sheet (h_{cs}) was slightly less than during the C10 flyby, the magnitude of the induced magnetic moment for C21 ($|\mathbf{M}_{ind}| = 1.96 \cdot 10^{18}$ Am^2) is approximately 80% of the induced moment during C10. Inserting the C21 magnetic moment into equation (1) results in a peak induced field strength of $|\mathbf{B}_{ind,max}| = 28.4$ nT on the surface of Callisto (at its magnetic poles), with $\mathbf{B}_{ind,max} = \left[5.0\hat{\mathbf{x}} - 28.0\hat{\mathbf{y}} + 0.0\hat{\mathbf{z}}\right]$ nT.

Hence, at the C/A altitude of the C21 flyby ($d_{C/A} = 0.43\,R_C$), the r^{-3} dependence of the induced dipole field would yield a maximum perturbation of $\delta B_{x,max} = 1.69$ nT above the magnetic poles of Callisto. However, C/A of the C21 flyby occurred in the magnetic equatorial plane of Callisto's induced dipole (i.e., near the intersection of the trajectory with the x axis; see Figure 4), where the induced field is nearly a factor of 2 weaker than

the maximum value near the magnetic poles. The magnetic field signatures generated by the induced dipole along the C21 trajectory are included in Figure 3a in blue and are clearly much weaker than the observed field perturbations. In addition to the *magnitudes* of the dipole-generated δB_x and δB_y features being too weak, the *orientation* of the induced magnetic field in the moon's plasma shadow is not consistent with the observed perturbations either.

If the measured δB_x and δB_y signatures in Callisto's geometric plasma shadow were related to the induced field, they must therefore have been generated through "stretching" of the dipole field into the wake due to the plasma interaction. If such a deformation were able to explain the *observed* δB_x enhancement of nearly 30 nT, the maximum δB_x generated by the pure dipole along C21 ($\delta B_x = 0.85$ nT) would have to be enhanced by a factor of 35. Such strong stretching of the wakeside dipolar field is implausible at close distances to Callisto, especially since it is not consistent with magnetic field observations and modeling of the moon's plasma interaction during the C10 flyby [*Liuzzo et al.*, 2016]. Hence, although qualitatively similar B_x perturbations were detected during C10 and C21, deformation of the moon's induced dipole could not have generated the perturbation signatures measured in Callisto's geometric plasma shadow during C21.

We now investigate whether the plasma interaction with Callisto's ionosphere and induced dipole could have generated the observed magnetic perturbations, particularly in B_x. A schematic of the expected δB_x signatures in Callisto's equatorial plane is displayed in Figure 4b. Jovian field lines frozen into the (nearly) corotating magnetospheric plasma pile up on the ramside ($x < 0$) of Callisto and drape around the moon's (yellow) ionosphere and (magenta) induced dipole. Farther from Callisto, the draped field lines form Alfvén wings, resulting in $\delta B_x < 0$ in the moon's Jupiter-averted ($y < 0$) hemisphere and $\delta B_x > 0$ in its Jupiter-facing ($y > 0$) hemisphere. The large C/A altitude of C21 prevented Galileo from sampling the quasi-dipolar core region downstream of Callisto (see Figure 4b). This is also visible in Figure 3b, which shows that this region only extended approximately $0.2\,R_C$ above the moon's wakeside surface. Therefore, the spacecraft, with its closest approach altitude of $d_{C/A} = 0.43\,R_C$, did not intersect this region.

Represented by the dark green lines in Figure 3a are the magnetic perturbations along the C21 trajectory from a hybrid simulation with an upstream flow velocity of $\mathbf{u}_0 = u_0\hat{\mathbf{x}}$ and $u_0 = 320$ km/s (denoted corotational in Table 2). Inbound of Callisto's geometric plasma shadow, the modeled $\delta B_x < 0$ feature corresponds to draped field lines in the moon's Jupiter-averted (northern, $\mathcal{Z}^-$) Alfvén wing, which is also visible in Figure 3b. However, although the model shows qualitatively similar signatures as the data within this region, the modeled perturbation of $\delta B_x \approx -16$ nT is nearly three times as strong as the measured perturbation. Additionally, the decrease in B_x would have been encountered much earlier in the model (before 07:30) compared to the actual observation (near 07:35).

Outbound of Callisto's geometric plasma shadow, the hybrid model (dark green line in Figure 3a) suggests a passage through the moon's Jupiter-facing (southern, $\mathcal{Z}^+$) Alfvén wing, with a peak perturbation of $\delta B_x \approx 24$ nT near 07:53. During the C21 flyby, a $\delta B_x > 0$ signature of similar magnitude was observed *within* Callisto's geometric plasma shadow. However, this region of measured $\delta B_x > 0$ had a spatial extension of less than $1.3\,R_C$ along the C21 trajectory and was confined entirely to Callisto's plasma shadow, whereas the region of modeled $\delta B_x > 0$ extends out of the shadow for more than $6\,R_C$ into the Jupiter-facing hemisphere (see also Figure 3b). The modeled $\delta B_x < 0$ feature inbound of Callisto's plasma shadow (corresponding to the Jupiter-averted wing) gradually transitions to the modeled $\delta B_x > 0$ feature outbound of the shadow (corresponding to the Jupiter-facing wing). Thus, the results of the simulation suggest that Callisto's plasma interaction is indeed able to produce a $\delta B_x > 0$ of the same magnitude as the observed perturbation. However, this simulation produces a broad enhancement in B_x and is not able to explain the alternating signs of the observed B_x perturbations.

Only in the center of Callisto's geometric plasma shadow the modeled orientation and strength of the $\delta B_y < 0$ signature (dark green line in Figure 3a) are similar to the perturbation of $\delta B_y \approx -15$ nT observed by Galileo in this region. However, Galileo detected regions of $\delta B_y > 0$ inbound and outbound of the plasma shadow, whereas the hybrid model rather suggests a broad decrease of B_y without any fine structure in these regions. Figure 3c shows the modeled δB_y in Callisto's equatorial ($z = 0$) plane for the corotational run, with the expected pileup region visible at the moon's ramside. Downstream of Callisto, the modeled reduction of B_y "fills" the moon's entire wake region.

The nearly featureless regions in δB_z observed during the C21 encounter inbound and outbound of Callisto's plasma shadow are represented by the hybrid model (dark green line in Figure 3a) reasonably well. The most

important structure that is distinctly different between model and data is the "pillar" of $\delta B_z > 0$ that was observed near closest approach, from 07:46 to 07:49 (highlighted in turquoise in Figure 3a). In this region, B_z locally increased by more than 20 nT. The feature coincides with the second half of the M-like B_x increase observed within Callisto's geometric plasma shadow. Similarly correlated enhancements in B_x and B_z were also seen in Callisto's plasma shadow during the C10 flyby. *Liuzzo et al.* [2016] attributed the spike observed during C10 to one of two possible sources: the first could have been the presence of a narrow filament of escaping plasma from Callisto's ionosphere, similar to the transient channels of escaping ions observed in Titan's wake during the Cassini T9, T63, and T75 flybys [*Coates et al.*, 2012; *Feyerabend et al.*, 2015]. Alternatively, the narrow spikes in B_x and B_z could have been magnetospheric in origin and therefore unassociated with Callisto's plasma interaction.

For the C21 flyby, the hybrid model predicts a localized enhancement in ionospheric O_2^+ density at the outbound edge of Callisto's geometric plasma shadow, as visible in Figure 3d. The model shows an O_2^+ number density increase by more than 2 orders of magnitude in the region where the pillar-like δB_z feature was observed. However, despite the modeled increase in ionospheric plasma density at this location, no simulation within the parameter regime explored was able to generate a strong and localized magnetic response in B_z at the same position. Our ionosphere model represents only the "average" state of Callisto's ionosphere and therefore cannot account for transient, localized outflow events during a single flyby. We also note that the most comprehensive ionosphere model available for Callisto [*Hartkorn et al.*, 2017] does not display any localized inhomogeneities that could produce such a narrow magnetic response (see Figure 10 in that work).

Overall, the mechanism that could be responsible for generation of a strong B_x enhancement in Callisto's entire plasma shadow is still unclear. As shown in Figures 3a, 3b, and 4b, the only feature associated with Callisto's plasma interaction that would be able to produce a positive δB_x of comparable magnitude is the moon's Jupiter-facing (southern) Alfvén wing. However, the modeled wing is sampled at a location along the C21 trajectory that is inconsistent with the actual Galileo observation. One way to partially shift the Jupiter-facing wing into Callisto's plasma shadow is through an upstream flow $\mathbf{u}_0$ pointing away from Jupiter:

$$\mathbf{u}_0 = u_0 \left[\cos(\xi)\hat{\mathbf{x}} - \sin(\xi)\hat{\mathbf{y}} \right] , \qquad (5)$$

where $\xi > 0$ is the angle between the upstream flow velocity and the corotation direction (aligned with $\hat{\mathbf{x}}$). Such a noncorotational flow would "rotate" the Alfvén wing characteristics (see equation (4)) clockwise around Callisto, and as a result, the Jupiter-facing wing (along with its associated $\delta B_x > 0$ perturbation) would penetrate into the moon's plasma shadow.

This effect has actually been observed by the Cassini spacecraft during the T9 wakeside flyby of Titan [*Bertucci et al.*, 2007], and several hybrid models have successfully reproduced the associated magnetic field perturbations [*Simon et al.*, 2007; *Modolo et al.*, 2007; *Kallio et al.*, 2007]. We therefore use this as a working hypothesis for the C21 flyby, especially since tentative analysis of plasma observations near Callisto indicates that the upstream magnetospheric flow direction may occasionally deviate from the corotation direction [see *Seufert*, 2012, Table 3.2]. Although the survey of Galileo plasma data by *Bagenal et al.* [2016] intentionally excluded the times surrounding the Callisto encounters, their results are generally consistent with a nonnegligible radial flow component in Jupiter's middle magnetosphere (see Figures 3, 5, 7, and 8 in that work). This may further substantiate our hypothesis of a rotated upstream flow for C21. A schematic of the resulting interaction is given in Figure 4c, where a nonzero component of the flow vector $\mathbf{u}_0$ away from Jupiter is able to partially place Callisto's Jupiter-facing Alfvén wing into the moon's geometric plasma shadow.

Multiple simulations using various angles ξ have been performed with the goal of rotating Callisto's Jupiter-facing Alfvén wing to the location of the observed $\delta B_x > 0$ within the plasma shadow. We have found that an angle of $\xi \approx 50°$ (see equation (5)) is best suitable to meet this requirement for C21. Smaller angles fail to rotate the wing far enough into the plasma shadow, whereas much larger angles weaken the B_x perturbation along the C21 trajectory too drastically to be detectable above the background field. Additionally, we tested the effect of a nonzero component of $\mathbf{u}_0$ along the $\pm\hat{\mathbf{z}}$ directions. Such a north/south aligned flow component reduces the cross section of the wing along the spacecraft trajectory. Hence, the B_x perturbation has a more narrow spatial extension which would be compatible with the actual data. However, this also reduces the magnitude of the B_x perturbation to much lower than the observed value.

Simulation results from the hybrid model with $\xi = 50°$ (denoted noncorotational in Table 2) are represented by the red lines in Figure 3a. As expected, the modeled $\delta B_x > 0$ feature is now rotated to fill Callisto's plasma

shadow, with the peak magnitude of the modeled enhancement still roughly consistent with the observed δB_x. The Jupiter-facing wing is visible in Figure 3e and penetrates much deeper into Callisto's geometric plasma shadow than in the corotational run (cf. Figure 3b). Additionally, the peak magnitude of the B_x perturbation in this wing is now slightly reduced due to the asymmetry of the draping pattern [see *Simon and Motschmann*, 2009]. However, the modeled $\delta B_x > 0$ is still much broader (extending more than 7 R_C along the spacecraft trajectory) than the observed perturbation (with an extension of less than 1.3 R_C).

The modeled B_y (see also Figure 3f) and B_z perturbations along the C21 trajectory are fairly robust against the rotation of $\mathbf{u}_0$: only small quantitative differences are present compared to the corotational run (see Figure 3a). Additionally, the ionospheric O_2^+ tail structure, visible in Figure 3g, is similar between the two simulations: outflow is mainly confined to a narrow channel downstream of Callisto, since ion gyration takes place nearly perpendicular to the $z = 0$ plane. However, while the picked up ionospheric particles still accumulate in the narrow $\delta B_x \approx 0$ region of Callisto's magnetotail (white in Figures 3b and 3e), this region is now rotated into Callisto's Jupiter-averted ($y < 0$) hemisphere.

In summary, the noncorotational simulation demonstrates that Callisto's steady state plasma interaction can generate a B_x enhancement of the observed magnitude directly downstream of the moon. In this case, the plasma interaction model also predicts the observed $\delta B_y < 0$ reduction in the plasma shadow reasonably well. Despite this, there are also numerous observed features which are not consistent with Callisto's steady state plasma interaction, especially the alternating signs of the perturbations in B_x and B_y.

Hence, the steady state plasma interaction only partially completes our understanding of Callisto's magnetic environment during the C21 flyby. We therefore suggest that the remaining magnetic features may rather be generated by other mechanisms, including transient magnetospheric events. For instance, a short-lived plasma density enhancement near Callisto (e.g., due to the passage of a "blob" of plasma from Io traveling radially outward) could highly perturb the moon's local magnetospheric environment. Such an event has been observed, e.g., during the Galileo E12 flyby Europa on 16 December 1997. During the E12 flyby the magnetospheric plasma density near Europa exceeded 900 cm^{-3}, which is a factor of 9 higher than the maximum density expected from System III longitude variations [*Kurth et al.*, 2001]. This unusual plasma environment generated magnetic field perturbations during E12 that were nearly 90% of the background field magnitude, compared to other Europa flybys where perturbations on the order of only 10% of the background field were measured [*Kivelson et al.*, 1999].

Similarly, the magnetic perturbations observed during C21 were much stronger than those detected during any other Callisto flyby. It is therefore possible that at the time of C21, Callisto was interacting with an enhanced, nonstationary flux of magnetospheric plasma which partially caused these unusual magnetic field signatures. The idea of an Iogenic plasma blob passing Callisto during C21 is even consistent with our finding that a radial flow component away from Jupiter slightly improves agreement between the modeled and measured magnetic field (even though the fine structures in B_x and B_y remain unresolved).

4.3. The C23 Flyby

The C23 flyby of Callisto occurred on 16 September 1999. During this encounter Galileo passed within $d_{C/A} = 1052.3$ km $= 0.44 R_C$ of the moon's surface. For the first time since the C3 flyby on 4 November 1996, Callisto was located slightly north of the center of the Jovian magnetospheric current sheet during an encounter, with $h_{cs} = 0.87 R_J$. Because Callisto was located close to the center of the sheet, the magnetic signatures generated by induction are expected to be weak compared to those of the plasma interaction. As visible in Figure 1, the C23 trajectory was nearly identical to that of C22: Galileo traveled from Callisto's Jupiter-facing hemisphere ($y > 0$) into its Jupiter-averted hemisphere ($y < 0$) while located near the $z = 0$ plane.

Figure 5a displays the B_x, B_y, and B_z components as well as the magnitude $|\mathbf{B}|$ of the magnetic field measured during the C23 encounter (black). At closest approach to Callisto, the magnetospheric background field was approximately $\mathbf{B}_0 = [0.0\hat{\mathbf{x}} - 22.0\hat{\mathbf{y}} - 10.0\hat{\mathbf{z}}]$ nT, with $|\mathbf{B}_0| = 24.2$ nT. In the outbound segment of the C23 trajectory when Galileo was approximately 4 R_C from Callisto, the spacecraft crossed Jupiter's magnetic equatorial plane from north to south (shortly after 17:49, as indicated by the minimum of $|\mathbf{B}|$). This crossing was also visible in the B_y component, which changed from negative to positive values around 17:59. Around 17:45, the sign of B_x changed as well: since Jupiter's equatorial plasma sheet sub-corotates, the magnetic field lines in the sheet are swept back with respect to strictly corotating (magnetic) meridional planes. This causes
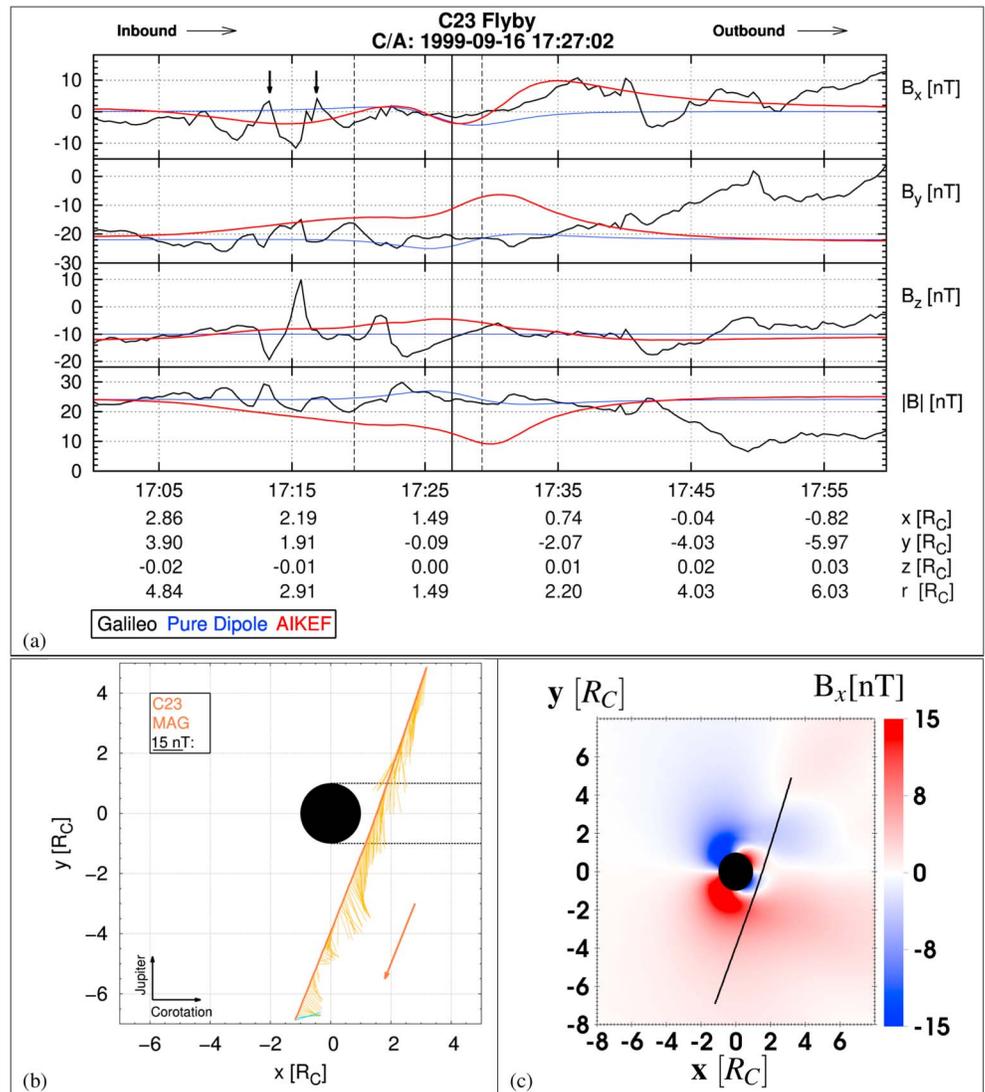
Figure 5. (a) From top to bottom: B_x, B_y, B_z, and $|\mathbf{B}|$ measured along the C23 flyby depicted by black lines. The purely dipolar inductive response of Callisto's subsurface ocean along the flyby trajectory is represented by the blue lines, and the hybrid model results are depicted in red. Vertical lines are as in Figures 2a and 3a. The two vertical arrows near 17:13 and 17:17 denote "interruptions" of Callisto's Jupiter-facing (northern) Alfvén wing and are discussed further in the text. (b) Measured magnetic field vectors along the C23 trajectory projected onto the $z = 0$ plane, with dotted bold lines denoting the outer edges of Callisto's geometric plasma shadow. During the flyby, Galileo was located (gold, $B_y < 0$) north and subsequently (light blue, $B_y > 0$) south of Jupiter's magnetic equatorial plane, with the crossing visible at the very end of the data interval shown here. The magnetic field vectors are plotted every 24 s. (c) Two-dimensional plot of the modeled B_x from the hybrid simulation in Callisto's equatorial ($z = 0$) plane.

$B_x < 0$ above and $B_x > 0$ below the magnetic equator [see, e.g., *Hill*, 1979; *Khurana and Kivelson*, 1993]. The field magnitude $|\mathbf{B}|$ (see Figure 5a) decreased by more than a factor of 2 during the crossing. These changes in the background field $\mathbf{B}_0$ were much stronger than the perturbations detected closer to Callisto's geometric plasma shadow that may have been associated with the moon's magnetospheric interaction.

The reversals in the signs of B_x and B_y are slightly displaced with respect to the minimum of $|\mathbf{B}|$. However, this displacement is on the order of a few Callisto radii; i.e., it is negligible on magnetospheric length scales. This weak displacement may be caused by the warping of the magnetospheric current sheet which is already discernible near the orbit of Callisto [see, e.g., *Seufert et al.*, 2011, Figure 1A]. A local north-south asymmetry in the plasma density of the magnetodisk may also cause a slight asymmetry of the sweepback effect between both hemispheres.

The observed magnetic signatures near Callisto included a sequence of alternating dips and spikes in B_x from 17:08 to 17:23, with fluctuations between $B_x \approx -10$ nT and $B_x \approx +4$ nT. The average field in this region was $\langle B_x \rangle \approx -4$ nT; i.e., $\langle B_x \rangle$ was reduced compared to the background value of $B_{x,0} = 0$ nT. After Galileo exited Callisto's geometric plasma shadow, B_x was locally elevated for approximately $3\,R_C$ from 17:32 to 17:40, with a maximum of $B_x \approx +10$ nT. The B_y component was dominated by the magnetic equator crossing, while B_z remained nearly constant around $B_z \approx -10$ nT. Only a narrow, spiky increase less than $1\,R_C$ in width was observed in B_z around 17:15, with a maximum of $B_z \approx 10$ nT.

We estimate the contribution of Callisto's induced dipole to these magnetic signatures by inserting $\mathbf{B}_0$ into equation (2). This yields an induced magnetic moment of $\mathbf{M}_{ind} = \left[0.0\hat{\mathbf{x}} + 1.5\hat{\mathbf{y}}\right] \cdot 10^{18}$ Am^2 during the C23 flyby, which results in a maximum induced field strength of only $|\mathbf{B}_{ind,max}| \approx 4$ nT along the flyby trajectory (blue line in Figure 5a). This value is comparable in strength to the local fluctuations in the magnetospheric background field that were observed throughout the flyby; i.e., the C23 magnetometer data do not contain a clearly discernible induction signature.

As the induced dipole during C23 was not strong enough to generate the magnetic signatures observed around Callisto's geometric plasma shadow, we have performed multiple simulations (with different sets of upstream conditions) to determine whether these perturbations can be explained by Callisto's plasma inter-action. The red lines in Figure 5a display the hybrid model results using the magnetospheric background parameters from Table 2. Combining the background field $\mathbf{B}_0$ at closest approach with an upstream number density of $n_0 = 0.3$ cm^{-3} and velocity of $\mathbf{u}_0 = u_0\hat{\mathbf{x}}$ and $u_0 = 192$ km/s yields a sub-Alfvénic ($M_A = 0.86$) plasma flow around Callisto, similar to during C22.

From equation (4), it follows that the Jupiter-facing (northern, $\mathcal{Z}^-$) and Jupiter-averted (southern, $\mathcal{Z}^+$) Alfvén wings are inclined against Callisto's equatorial ($z = 0$) plane at angles of approximately $+19°$ and $-19°$, respectively. Due to $B_{x,0} = 0$ nT and $\mathbf{u}_0$ aligned with $\hat{\mathbf{x}}$, the two wings are inclined against this plane by the same angle. The modeled Alfvén wings at Callisto's wakeside are visible in Figure 5c. Due to the inclination, the B_x perturbations weaken with increasing distance along the x axis. The slight asymmetry between the two wings can be attributed to the nonnegligible gyroradii of pickup ions near Callisto (see Table 2). As shown by *Liuzzo et al.* [2015] for a magnetospheric field with $B_{x,0} = 0$ nT and $\mathbf{u}_0$ aligned with $\hat{\mathbf{x}}$, field line draping is symmetric only in planes containing $\mathbf{B}_0$ and $\mathbf{u}_0$ but becomes more and more asymmetric with increasing inclination of the cutting plane against $\mathbf{B}_0$. Because the $z = 0$ plane was not parallel to $\mathbf{B}_0$ during C23, the draping pattern in this plane already exhibits a minor degree of asymmetry.

Along the C23 trajectory, the modeled Jupiter-facing wing is visible in B_x between 17:08 and 17:23 with a minimum perturbation of $B_x \approx -4$ nT (red line in Figure 5a, first panel). The modeled wing in the Jupiter-averted hemisphere is visible from 17:30 to 17:45, with a maximum perturbation of $B_x \approx +10$ nT. These differences in $|B_x|$ result from the slight asymmetry associated with ion gyration (see above discussion) as well as the inclination of the C23 trajectory with respect to the y axis. This inclination caused Galileo to pass through the Jupiter-averted wing (outbound) closer to Callisto where the B_x perturbations are stronger.

Our model results suggest that the B_x signatures observed inbound and outbound of Callisto's geometric plasma shadow were indeed generated by the moon's Alfvén wings. Outbound of the shadow, the magnitude of B_x observed within the wing is identical to that of the modeled wing ($B_x \approx 10$ nT). The extensions of the modeled and observed B_x perturbations in that region are also very similar, with the modeled Jupiter-averted wing only slightly broader than observed. For the Jupiter-facing wing, the modeled perturbation of $B_x \approx -4$ nT is consistent with the average perturbation of $\langle B_x \rangle \approx -4$ nT measured along the inbound segment of the trajectory. Additionally, the extensions of modeled and observed B_x perturbations (from 17:08 to 17:23, corresponding to approximately $0.75\,R_C$ along the flyby trajectory) are in very good agreement.

However, the model *does not* produce the observed short interruptions in the Jupiter-facing wing on the order of $B_x = 4$ nT, marked by the two vertical arrows in Figure 5a (first panel). It is possible that these interruptions were related to Jupiter's current sheet sweeping over Callisto and were a precursor to the upcoming magnetic equator crossing that occurred approximately 35 min later. This may also have been true for the isolated spike in B_z near 17:15. The Cassini spacecraft has detected similar magnetic perturbations in Saturn's magnetosphere as the giant planet's current sheet sweeps over Titan [e.g., *Simon et al.*, 2010]. Alternatively, the two interruptions of B_x in the Jupiter-facing wing may have been generated by localized inhomogeneities

of Callisto's ionospheric Pedersen and Hall conductances during C23 which mapped into the moon's Alfvén wing [see, e.g., *Neubauer*, 1998; *Simon*, 2015].

The observed B_y and B_z components show no discernible Callisto-related perturbations (see Figure 5a). The hybrid results are consistent with the observation of a nearly featureless B_z component during C23. The observed spike near 17:15 where B_z switched signs is not reproduced by the model, suggesting that this perturbation was indeed magnetospheric in origin and unrelated to Callisto. Additionally, in contrast to our C21 simulations, a rotation of the upstream flow velocity in Callisto's equatorial ($z = 0$) plane did not yield any improvement in agreement between model and data. In particular, such a rotation dislocated the modeled Jupiter-averted wing ($B_x > 0$, from 17:30 to 17:45) from the observed position.

The hybrid simulation is consistent with the B_y observations until near closest approach at 17:27. After C/A the hybrid model shows a B_y increase of more than 10 nT, caused by magnetic field line draping in Callisto's Jupiter-averted Alfvén wing and (to a much lesser extent) by contributions from the induced dipole. It is possible that during C23, the B_y signature of the Alfvén wings was obscured by the proximity to the Jovian magnetic equator crossing. However, a crossing of Jupiter's magnetic equator cannot be considered by our local simulation of Callisto's plasma environment, as such a crossing involves a nonnegligible change of $B_{x,0}$ (i.e., the magnetic field component aligned with the upstream flow direction). Such an effect cannot be included in *any* local plasma simulation model without violating the $\nabla \cdot \mathbf{B}_0 = 0$ condition [see *Simon et al.*, 2009; *Simon and Motschmann*, 2009; *Feyerabend et al.*, 2016].

Overall, our results indicate that Callisto's steady state plasma interaction alone is able to explain the observed Alfvén wing signatures in B_x. Despite the strong changes in the ambient magnetospheric field conditions during the flyby, Callisto was still "magnetically visible," especially in B_x where we were able to identify the moon's Alfvén wings in the magnetometer data. However, the C23 flyby is not suitable to impose further constraints on Callisto's subsurface ocean.

4.4. The C30 Flyby

The final Callisto flyby of the Galileo era, C30, occurred on 25 May 2001. During this last encounter, the spacecraft passed closer to Callisto's surface than during any other Galileo flyby, with a C/A altitude of only $d_{C/A} = 131.9$ km $= 0.05\,R_C$. Compared to the C23 flyby, Callisto was located even closer to the center of Jupiter's magnetospheric current sheet: during C30, the magnetic equator crossing nearly coincided with closest approach (see Figures 6a and 6b). Similar to the C22 and C23 flybys, Galileo traveled from Callisto's Jupiter-facing ($y > 0$) hemisphere into its Jupiter-averted ($y < 0$) hemisphere. On average, the spacecraft remained approximately $0.23\,R_C$ above the $z = 0$ plane (see Figure 1).

Depicted in Figure 6a is the measured magnetic field during the C30 flyby (black). The magnetometer data includes a gap from 11:18 to 11:20 (corresponding to $0.44\,R_C$ along the spacecraft trajectory), just as Galileo entered Callisto's geometric plasma shadow. In contrast to the other six Callisto flybys, the ambient magnetospheric field $\mathbf{B}_0$ during C30 was dominated by the north-south component. While Galileo was still within Callisto's geometric plasma shadow, the spacecraft passed through Jupiter's magnetic equator from south ($B_{y,0} > 0$) to north ($B_{y,0} < 0$) just after 11:25. This is also visible in Figure 6b which shows the observed magnetic field projected onto Callisto's equatorial plane before (depicted in light blue) and after (depicted in gold) the magnetic equator crossing. Along the inbound segment of the trajectory, $B_{x,0}$ was slightly positive due to the corotation lag [e.g., *Hill*, 1979]. However, the change in sign of $B_{x,0}$ that would be associated with a magnetic equator crossing occurred outside of the rather short time interval shown here.

Near closest approach to Callisto, Galileo detected a bipolar B_x signature. From 11:22 to 11:26, a positive B_x perturbation was observed with a maximum value of $B_x = 10$ nT. Subsequently, between 11:26 and 11:30, a negative B_x perturbation was detected with a minimum value of $B_x = -20$ nT. The orientation of the B_x perturbations in these regions is consistent with draping of the inbound magnetospheric field around Callisto. Since the inbound field had $B_{y,0} > 0$, draping would produce the observed B_x enhancement in the moon's Jupiter-facing hemisphere as well as the observed B_x decrease in its Jupiter-averted hemisphere. However, the observed *increase* in B_y before closest approach to a value of $B_y = 20$ nT is not consistent with field line draping, which would *reduce* B_y.

The region of enhanced B_x was "interrupted" by a discontinuity-like structure that was observed between 11:25:14 and 11:25:17 (highlighted in purple in Figure 6a). This discontinuity extended less than 54 km ($0.02\,R_C$) along the flyby trajectory and thus was even narrower than the rotational discontinuity detected

Figure 6. (a) Magnetic field components B_x, B_y, and B_z, along with $|\mathbf{B}|$ (black) measured by Galileo during the C30 Callisto encounter. Represented by the blue lines is the modeled magnetic field of a pure dipole induced within Callisto's subsurface ocean. There is a data gap between 11:18 and 11:20, and vertical lines are as in Figures 2a, 3a, and 5a. The (purple) discontinuity detected by Galileo at 11:25 is discussed in the text. (b) Measured magnetic field vectors during the C30 flyby, projected onto Callisto's equatorial plane. The vectors are plotted every 3 s. During the flyby, Galileo was located (light blue) south and subsequently (gold) north of Jupiter's magnetic equatorial plane. (c) Magnetic field vectors generated by a pure dipole induced within Callisto's subsurface ocean along the C30 trajectory, projected onto Callisto's equatorial plane. In Figures 6b and 6c, the dotted bold lines again denote the outer edges of Callisto's geometric plasma shadow.

in Callisto's geometric plasma shadow during the C10 flyby (which had an extension of approximately 0.09 R_C). During C10, the observed discontinuity separated the wakeside quasi-dipolar core region from the moon's Jupiter-facing Alfvén wing [*Liuzzo et al.*, 2016].

We have performed a minimum variance analysis [*Sonnerup and Cahill*, 1967] of the discontinuity seen during C30. The minimum, medium, and maximum eigenvalues of the variance matrix are λ_{min} = 0.1054, λ_{med} = 2.1151, and λ_{max} = 90.8239, respectively. These values yield a ratio between the minimum and medium eigenvalues of $\lambda_{min}/\lambda_{med}$ = 0.0498. The unit vector normal to the surface of the discontinuity was $\mathbf{e}_{min} = \left[0.4319\hat{\mathbf{x}} + 0.8926\hat{\mathbf{y}} + 0.1294\hat{\mathbf{z}}\right]$; i.e., it was aligned mainly with $\hat{\mathbf{y}}$ and also had a nonnegligible component toward downstream. Although these observations qualitatively resemble the discontinuity seen during C10, the C30 discontinuity *was not* rotational as $|\mathbf{B}|$ increased by 9 nT at its location. The origin of the narrow

structure observed during C30 is therefore unclear, but it may have been generated by dynamics of the neutral sheet between Callisto's magnetic lobes.

Denoted by the blue lines in Figure 6a are the magnetic signatures along the flyby trajectory that would be generated by an induced dipole. The associated magnetic moment $\mathbf{M}_{ind}$ has been obtained by using the background field along the inbound segment of the C30 trajectory (i.e., $\mathbf{B}_0 \approx \left[5.0\hat{\mathbf{x}} + 10.0\hat{\mathbf{y}} - 14.0\hat{\mathbf{z}}\right]$ nT). As can be seen, the induced field was much too weak to make appreciable contributions to the magnetic signatures measured during C30. The projection of the induced dipolar field (see equations (1) and (2)) onto Callisto's equatorial plane is shown in Figure 6c. By comparing the orientations of these vectors in Callisto's geometric plasma shadow with those in Figure 6b, it is clear that the induced dipole is not suitable to explain the measured perturbations. We also note that using the background magnetospheric field at closest approach to calculate $\mathbf{M}_{ind}$ would result in an even weaker induction signal, since $B_{y,0} \approx 0$ at that location. These findings again emphasize that the discontinuity observed during C30 *did not* separate the induced dipole from the draped magnetospheric field, in contrast to the discontinuity observed during C10.

No hybrid modeling results are included in this study for the C30 flyby. Because of the small C/A altitude of the encounter (see Figure 1), it is not possible to maintain a sufficient number of grid cells between Callisto's surface and the C30 trajectory while simultaneously using a domain large enough to exclude any impacts of the outer boundaries on the simulation results. Therefore, it is not feasible to provide reliable hybrid modeling results for C30 with current computing capacities.

Overall, magnetic field data from C30 show hints of field line draping and a discontinuity with a location and orientation similar to the discontinuity observed during C10. However, due to the moon's proximity to Jupiter's magnetic equator, the magnetometer data do not contain a discernible signature of induction from Callisto's subsurface ocean.

5. Summary and Concluding Remarks

This study has applied a combination of analytical modeling, hybrid simulations, and data analysis techniques to conduct an in-depth analysis of magnetometer data from the C21, C22, C23, and C30 Galileo flybys of Callisto. Accompanied by our two preceding studies [*Liuzzo et al.*, 2015, 2016], this work provides a comprehensive portrait of Callisto's magnetic environment based on data from all flybys during the Galileo era. Callisto was encountered at various distances to the center of the Jovian magnetospheric current sheet, ranging from far outside (as during C22, where $h_{cs} = -4.3\,R_J$) to within the center of the sheet (as during C23 and C30, where $h_{cs} = 0.9\,R_J$ and $h_{cs} = 0.0\,R_J$, respectively).

During all four of these flybys, Galileo detected clear signatures of field line draping/Alfvén wings at various strengths, partially obscured by ambient dynamics of the Jovian magnetosphere. However, magnetometer data obtained during these flybys showed no discernible induction signature from Callisto's subsurface ocean. Three effects contributed to the absence of measurable induction signals during C21, C22, C23, and C30:

1. Despite a "favorable" value of h_{cs}, strong plasma interaction signatures obscured the induced dipolar field (C21).
2. Although a strong induction signal was present, the C/A altitude of the flyby was too large for detection of the induced dipole (C22).
3. Callisto was located very close to Jupiter's magnetic equator where the inducing component of the magnetospheric background field nearly vanishes (C23, C30).

The results of this analysis, in combination with our two previous studies [*Liuzzo et al.*, 2015, 2016], provide constraints on the geometries of spacecraft flybys that are suitable to characterize Callisto's subsurface ocean based on magnetometer data alone. We thus classify the seven Galileo encounters of Callisto (where magnetic field measurements were taken) into three distinct groups. "First choice" flybys are highly suitable to confirm the existence and quantitatively characterize properties (i.e., conductivity, thickness, and depth) of Callisto's subsurface ocean. "Second choice" flybys are still suitable to identify Callisto's subsurface ocean in magnetometer data but also contain nonnegligible signatures generated by competing plasma effects (e.g., field line draping and pileup). These effects make it difficult to quantitatively constrain properties of the ocean. The remaining Galileo flybys that do not fit into either category are *not suitable* for detection of induction signatures associated with Callisto's subsurface ocean. This classification scheme is also helpful for planning and design of future missions (e.g., JUICE) that hope to characterize Callisto's subsurface ocean.

First choice flybys are those where Callisto is located far from the center of the Jovian magnetospheric current sheet and plasma currents are negligible. Therefore, the unobscured induction signal is clearly detectable in Callisto's ramside and wakeside hemispheres at altitudes well below 1 R_C. The two examples of first choice Galileo flybys are the wakeside C3 and ramside C9 encounters [e.g., *Khurana et al.*, 1998; *Kivelson et al.*, 1999; *Zimmer et al.*, 2000; *Liuzzo et al.*, 2015]. Despite the large distance of Callisto from the center of the Jovian current sheet during C22 (similar to C3 and C9), the C/A altitude of that flyby was too large (Table 1) for detection of the induction signal. In other words, although the location of Callisto with respect to the Jovian current sheet was favorable, the high closest approach altitude excludes C22 from the first choice flyby category.

Second choice flybys are those where Callisto is located closer to the center of Jupiter's magnetospheric current sheet; i.e., magnetic signatures associated with plasma currents (like field line draping and pileup) are nonnegligible. However, the induction signal still dominates Callisto's magnetic environment in the moon's geometric plasma shadow below altitudes of 1 R_C. While the induced dipole is visible at Callisto's wakeside, it is obscured at the ramside due to magnetic field pileup [*Liuzzo et al.*, 2016]. As long as a second choice flyby takes place under nominal, steady state upstream conditions, magnetic field data may at least confirm the existence (but not allow to refine existing constraints on properties) of Callisto's subsurface ocean. The one example of a second choice Galileo flyby is the wakeside C10 encounter [*Liuzzo et al.*, 2016]. Although the C21 flyby was similar to C10 in distance to the center of the Jovian magnetospheric current sheet and C/A altitude, atypical magnetospheric upstream conditions likely prevented identification of any induction signatures in observed magnetic field data.

In addition to C21 and C22, the C23 and C30 flybys were both *not suitable* for detection of Callisto's subsurface ocean due to the moon's close proximity to the center of the Jovian magnetospheric current sheet. Near the center of the sheet, plasma currents dominate Callisto's magnetic environment and the induction signatures are weak. For the upcoming JUICE mission, characterizing Callisto's subsurface ocean will therefore be most effective during future first choice or second choice flybys of the moon.

References

Bagenal, F., R. J. Wilson, S. Siler, W. R. Paterson, and W. S. Kurth (2016), Survey of Galileo plasma observations in Jupiter's plasma sheet, *J. Geophys. Res. Planets*, *121*, 871–894, doi:10.1002/2016JE005009.

Bertucci, C., F. M. Neubauer, K. Szego, J.-E. Wahlund, A. J. Coates, M. K. Dougherty, D. T. Young, and W. S. Kurth (2007), Structure of Titan's mid-range magnetic tail: Cassini magnetometer observations during the T9 flyby, *Geophys. Res. Lett.*, *34*, L24S02, doi:10.1029/2007GL030865.

Carlson, R. W. (1999), A tenuous carbon dioxide atmosphere on Jupiter's moon Callisto, *Science*, *283*(5403), 820–821, doi:10.1126/science.283.5403.820.

Coates, A. J., et al. (2012), Cassini in Titan's tail: CAPS observations of plasma escape, *J. Geophys. Res.*, *117*, A05324, doi:10.1029/2012JA017595.

Cunningham, N. J., J. R. Spencer, P. D. Feldman, D. F. Strobel, K. France, and S. N. Osterman (2015), Detection of Callisto's oxygen atmosphere with the Hubble Space Telescope, *Icarus*, *254*, 178–189.

Feyerabend, M., S. Simon, U. Motschmann, and L. Liuzzo (2015), Filamented ion tail structures at Titan: A hybrid simulation study, *Planet. Space Sci.*, *117*, 362–376.

Feyerabend, M., S. Simon, F. M. Neubauer, U. Motschmann, C. Bertucci, N. J. Edberg, G. B. Hospodarsky, and W. S. Kurth (2016), Hybrid simulation of Titan's interaction with the supersonic solar wind during Cassini's T96 flyby, *Geophys. Res. Lett.*, *43*, 35–42, doi:10.1002/2015GL066848.

Gurnett, D. A., W. S. Kurth, A. Roux, and S. J. Bolton (1997), Absence of a magnetic-field signature in plasma-wave observations at Callisto, *Nature*, *387*(6630), 261–262, doi:10.1038/387261a0.

Gurnett, D. A., A. M. Persoon, W. S. Kurth, A. Roux, and S. J. Bolton (2000), Plasma densities in the vicinity of Callisto from Galileo plasma wave observations, *Geophys. Res. Lett.*, *27*(13), 1867–1870, doi:10.1029/2000GL003751.

Hartkorn, O., J. Saur, and D. F. Strobel (2017), Structure and density of Callisto's atmosphere from a fluid-kinetic model of its ionosphere: Comparison with Hubble Space Telescope and Galileo observations, *Icarus*, *282*, 237–259.

Hill, T. W. (1979), Inertial limit on corotation, *J. Geophys. Res.*, *84*(A11), 6554–6558, doi:10.1029/JA084iA11p06554.

Kallio, E., I. Sillanpää, R. Jarvinen, P. Janhunen, M. Dougherty, C. Bertucci, and F. Neubauer (2007), Morphology of the magnetic field near Titan: Hybrid model study of the Cassini T9 flyby, *Geophys. Res. Lett.*, *34*, L24S09, doi:10.1029/2007GL030827.

Khurana, K. K., and M. G. Kivelson (1993), Inference of the angular velocity of plasma in the Jovian magnetosphere from the sweepback of magnetic field, *J. Geophys. Res.*, *98*, 67–79, doi:10.1029/92JA01890.

Khurana, K. K., M. G. Kivelson, C. T. Russell, R. J. Walker, and D. J. Southwood (1997), Absence of an internal magnetic field at Callisto, *Nature*, *387*(6630), 262–264, doi:10.1038/387262a0.

Khurana, K. K., M. G. Kivelson, D. J. Stevenson, G. Schubert, C. T. Russell, R. J. Walker, and C. Polanskey (1998), Induced magnetic fields as evidence for subsurface oceans in Europa and Callisto, *Nature*, *395*(6704), 777–780, doi:10.1038/27394.

Kivelson, M. G. (2004), Moon–magnetosphere interactions: A tutorial, *Adv. Space Res.*, *33*(11), 2061–2077.

Kivelson, M. G., K. K. Khurana, D. J. Stevenson, L. Bennett, S. Joy, C. T. Russell, R. J. Walker, C. Zimmer, and C. Polanskey (1999), Europa and Callisto: Induced or intrinsic fields in a periodically varying plasma environment, *J. Geophys. Res.*, *104*(A3), 4609–4626, doi:10.1029/1998JA900095.

Kivelson, M. G., F. Bagenal, W. S. Kurth, F. M. Neubauer, C. Paranicas, and J. Saur (2004), Magnetospheric interactions with satellites, in *Jupiter. The Planet, Satellites and Magnetosphere*, edited by M. G. Kivelson et al., pp. 513–536, Cambridge Univ. Press, Cambridge, U. K.

Kliore, A. J., A. Anabtawi, R. G. Herrera, S. W. Asmar, A. F. Nagy, D. P. Hinson, and F. M. Flasar (2002), Ionosphere of Callisto from Galileo radio occultation observations, *J. Geophys. Res.*, *107*, 1407, doi:10.1029/2002JA009365.

Kriegel, H., S. Simon, U. Motschmann, J. Saur, F. M. Neubauer, A. M. Persoon, M. K. Dougherty, and D. A. Gurnett (2011), Influence of negatively charged plume grains on the structure of Enceladus' Alfvén wings: Hybrid simulations versus Cassini MAG data, *J. Geophys. Res.*, *116*, A10223, doi:10.1029/2011JA016842.

Kriegel, H., S. Simon, P. Meier, U. Motschmann, J. Saur, A. Wennmacher, D. F. Strobel, and M. K. Dougherty (2014), Ion densities and magnetic signatures of dust pick-up at Enceladus, *J. Geophys. Res. Space Physics*, *119*, 2740–2774, doi:10.1002/2013JA019440.

Kurth, W. S., D. A. Gurnett, A. M. Persoon, A. Roux, S. J. Bolton, and C. J. Alexander (2001), The plasma wave environment of Europa, *Planet. Space Sci.*, *49*, 345–363, doi:10.1016/S0032-0633(00)00156-2.

Ledvina, S. A., S. H. Brecht, and T. E. Cravens (2012), The orientation of Titan's dayside ionosphere and its effects on Titan's plasma interaction, *Earth Planets Space*, *64*, 207–230.

Lindkvist, J., M. Holmström, K. Khurana, S. Fatemi, and S. Barabash (2015), Callisto plasma interactions: Hybrid modeling including induction by a subsurface ocean, *J. Geophys. Res. Space Physics*, *120*, 4877–4889, doi:10.1002/2015JA021212.

Liuzzo, L., M. Feyerabend, S. Simon, and U. Motschmann (2015), The impact of Callisto's atmosphere on its plasma interaction with the Jovian magnetosphere, *J. Geophys. Res. Space Physics*, *120*, 9401–9427, doi:10.1002/2015JA021792.

Liuzzo, L., S. Simon, M. Feyerabend, and U. Motschmann (2016), Disentangling plasma interaction and induction signatures at Callisto: The Galileo C10 flyby, *J. Geophys. Res. Space Physics*, *121*, 8677–8694, doi:10.1002/2016JA023236.

Modolo, R., G. M. Chanteur, J.-E. Wahlund, P. Canu, W. S. Kurth, D. Gurnett, A. P. Matthews, and C. Bertucci (2007), Plasma environment in the wake of Titan from hybrid simulation: A case study, *Geophys. Res. Lett.*, *34*, L24S07, doi:10.1029/2007GL030489.

Müller, J., S. Simon, U. Motschmann, J. Schüle, K. Glassmeier, and G. J. Pringle (2011), A.I.K.E.F.: Adaptive hybrid model for space plasma simulations, *Comput. Phys. Commun.*, *182*(4), 946–966, doi:10.1016/j.cpc.2010.12.033.

Neubauer, F. M. (1980), Nonlinear standing Alfvén wave current system at Io: Theory, *J. Geophys. Res.*, *85*, 1171–1178, doi:10.1029/JA085iA03p01171.

Neubauer, F. M. (1998), The sub-Alfvénic interaction of the Galilean satellites with the Jovian magnetosphere, *J. Geophys. Res.*, *103*, 19,843–19,866, doi:10.1029/97JE03370.

Neubauer, F. M. (1999), Alfvén wings and electromagnetic induction in the interiors: Europa and Callisto, *J. Geophys. Res.*, *104*, 28,671–28,684, doi:10.1029/1999JA900217.

Richards, P. C., J. A. Fennelly, and D. G. Torr (1994), EUVAC: A solar EUV flux model for aeronomic calculations, *J. Geophys. Res.*, *99*, 8981–8992.

Rubin, M., et al. (2015), Self-consistent multifluid MHD simulations of Europa's exospheric interaction with Jupiter's magnetosphere, *J. Geophys. Res. Space Physics*, *120*, 3503–3524, doi:10.1002/2015JA021149.

Seufert, M. (2012), Callisto: Induction signals, atmosphere and plasma interaction, PhD thesis, Univ. zu Köln. [Available at http://kups.ub.uni-koeln.de/4903.]

Seufert, M., J. Saur, and F. M. Neubauer (2011), Multi-frequency electromagnetic sounding of the Galilean moons, *Icarus*, *214*(2), 477–494, doi:10.1016/j.icarus.2011.03.017.

Simon, S. (2015), An analytical model of sub-Alfvénic moon-plasma interactions with application to the hemisphere coupling effect, *J. Geophys. Res. Space Physics*, *120*, 7209–7227, doi:10.1002/2015JA021529.

Simon, S., and U. Motschmann (2009), Titan's induced magnetosphere under non-ideal upstream conditions: 3D multi-species hybrid simulations, *Planet. Space Sci.*, *57*, 2001–2015, doi:10.1016/j.pss.2009.08.010.

Simon, S., G. Kleindienst, A. Boesswetter, T. Bagdonat, U. Motschmann, K.-H. Glassmeier, J. Schuele, C. Bertucci, and M. K. Dougherty (2007), Hybrid simulation of Titan's magnetic field signature during the Cassini T9 flyby, *Geophys. Res. Lett.*, *34*(L24S08), doi:10.1029/2007GL029967.

Simon, S., U. Motschmann, G. Kleindienst, J. Saur, C. Bertucci, M. Dougherty, C. Arridge, and A. Coates (2009), Titan's plasma environment during a magnetosheath excursion: Real-time scenarios for Cassini's T32 flyby from a hybrid simulation, *Ann. Geophys.*, *27*, 669–685.

Simon, S., A. Wennmacher, F. Neubauer, C. Bertucci, H. Kriegel, J. Saur, C. Russell, and M. Dougherty (2010), Titan's highly dynamic magnetic environment: A systematic survey of Cassini magnetometer observations from flybys TA–T62, *Planet. Space Sci.*, *58*, 1230–1251, doi:10.1016/j.pss.2010.04.021.

Simon, S., J. Saur, H. Kriegel, F. Neubauer, U. Motschmann, and M. Dougherty (2011), Influence of negatively charged plume grains and hemisphere coupling currents on the structure of Enceladus' Alfvén wings: Analytical modelling of Cassini magnetometer observations, *J. Geophys. Res.*, *116*, A04221, doi:10.1029/2010JA016338.

Smith, E. J., L. Davis, D. E. Jones Jr., P. J. Coleman Jr., D. S. Colburn, P. Dyal, C. P. Sonett, and A. M. A. Frandsen (1974), The planetary magnetic field and magnetosphere of Jupiter: Pioneer 10, *J. Geophys. Res.*, *79*, 3501–3513, doi:10.1029/JA079i025p03501.

Smith, E. J., L. Davis, D. E. Jones Jr., P. J. Coleman Jr., D. S. Colburn, P. Dyal, and C. P. Sonett (1975), Jupiter's magnetic field. Magnetosphere, and interaction with the solar wind: Pioneer 11, *Science*, *188*(4187), 451–455.

Sonnerup, B. U. O., and L. J. Cahill (1967), Magnetopause structure and attitude from Explorer 12 observations, *J. Geophys. Res.*, *72*(1), 171–183, doi:10.1029/JZ072i001p00171.

Strobel, D. F., J. Saur, P. D. Feldman, and M. A. McGrath (2002), Hubble Space Telescope Space Telescope Imaging Spectrograph search for an atmosphere on Callisto: A Jovian unipolar inductor, *Astrophys. J.*, *581*(1), L51–L54, doi:10.1086/345803.

Volwerk, M., K. Khurana, and M. Kivelson (2007), Europa's Alfvén wing: Shrinkage and displacement influenced by an induced magnetic field, *Ann. Geophys.*, *25*(4), 905–914.

Zimmer, C., K. K. Khurana, and M. G. Kivelson (2000), Subsurface oceans on Europa and Callisto: Constraints from Galileo magnetometer observations, *Icarus*, *147*(2), 329–347, doi:10.1006/icar.2000.6456.